ABSTRACT

Title of thesis	**Construction of Test Facility To Measure And Visualize Refrigerant Maldistribution in Multiport Evaporator Headers**
Degree Candidate	John Linde
Degree and Year	Master of Science, 2005
Thesis directed by	Professor Reinhard Radermacher, Ph.D. Department of Mechanical Engineering

In a refrigeration cycle, condensed liquid refrigerant is expanded to a two-phase fluid entering the evaporator. In many applications, the evaporator paths are divided into a number of parallel sections to keep the pressure drop across the evaporator within a reasonable range and to maximize overall heat exchanger performance. Since the state of the refrigerant entering the evaporator is two-phase and its quality changes depending upon the operating conditions, the proper refrigerant distribution to individual sections is not an easy task. Nonuniform distribution, or maldistribution, will cause dry out at sections of lesser mass flow by superheating the refrigerant gas. This can result in nonuniform heat exchanger surface temperature distribution. Single-phase heat transfer coefficients (HTCs) are much lower than those of two-phase HTCs. When dryout occurs, both refrigerant-side HTCs and air-side HTCs are lower than those of wet surfaces. In addition to this, the temperature difference between the air and refrigerant decreases due to the increased refrigerant temperature. Therefore, refrigerant maldistribution results in an overall deterioration of heat exchanger performance.

The main goal of this work is to construct a test facility to visualize and measure the two-phase refrigerant flow through a multiport header of a flat multiport tube (FMT) heat exchanger and to investigate maldistribution. Using a transparent test section, a better understanding of the flow behavior will be obtained. The test facility should also measure the mass and vapor quality distribution in the multiport header, using a combination of energy balances and physical measurements.

Most previous two-phase flow distribution studies investigated plate or serpentine exchangers. FMT heat exchangers have different geometries, and need to be studied independently. It is the objective of this work to provide essential design information for FMT evaporators by constructing an experimental setup which measures the effects of geometry, operating conditions, and fluid properties on both the distribution of liquid refrigerant and pressure drop across FMT heat exchangers.

CONSTRUCTION OF A TEST FACILITY TO MEASURE AND VISUALIZE REFRIGERANT MALDISTRIBUTION IN MULTIPORT EVAPORATOR HEADERS

By

John Eric Linde, IV

Thesis submitted to the Faculty of the Graduate School of the
University of Maryland, College Park in partial fulfillment
of the requirements for the degree of
Master of Science
2005

Advisory Committee:

Professor Reinhard Radermacher
Associate Professor Jungho Kim
Assistant Professor Elias Balaras

Dedication

This is lovingly dedicated to my parents and Aziza, for the endless love, support, and encouragement they gave to make this work possible.

Acknowledgement

I would like to first extend my thanks to my advisor, Dr. Reinhard Radermacher, for giving me the opportunity to pursue this degree. I also would like to thank Dr. Yunho Hwang for his advice, guidance, and the time he spent with my project.

I am indebted to all the people at the University of Maryland who have given so freely of themselves to help me in my endeavors. Many thanks to my current and former colleagues, notably Layla Monajemi, Mark Treadwell, Lorenzo Cremaschi, Jan Mühlbauer, James Kalinger, Ahmet Örs, Xudong Wang, Alexander Büchele, Joshua Dinaburg, Amr Gado, Hans-Joachim Huff, Dae-Hyun Jin, Renate Müller, Aydin Çelik, and the students of CHP and ISOC. I couldn't have done it without you, and I wish you all the best.

In addition to the students of CEEE, there are also some individuals who made a world of difference in my work who I want to thank: Howard Grossenbacher of the Machine Shop, for his invaluable, knowledgeable, and always entertaining instruction and assistance in machining and design. Bob Woodworth of the Physics Materials Store, whose skills in acquiring materials, answers, and low prices are unparalleled. Brian Cugle and Bill Grubb, who helped me through many a logistical puzzle with class and humor. Penny Komsat and Lita Brown, for handling the business side of my project, and all its headaches. All of you have my sincere and eternal gratitude for your assistance in my project.

Outside of work, I want to thank the people who kept me sane in the face of 75 hour work weeks and all the other joys of graduate school. This was no small feat, so to all my friends at CEEE, and from Penn State, Metzerott Rd, Habitat for Humanity, York, ASHRAE, and UMD – thank you, thank you, thank you. Aziza, thank you for the counsel, love, support, and friendship you have given so freely. I owe you the world.

Lastly, I want to thank my parents, family – Turkish and American. Your support helped through the toughest times of my life, and I love and thank you all. A kid simply couldn't ask for a better family than the one I have.

Table of Contents

1 Introduction

1.1 Overview

In refrigeration cycles, condensed liquid is expanded into a two-phase mixture at the inlet to the evaporator. In many applications, the evaporator is divided into a number of parallel sections to minimize the pressure drop across the evaporator, and to maximize overall heat exchanger performance. However, achieving an even distribution between the parallel sections is a difficult task due to the nature of two-phase mixtures. Also, the vapor quality of the mixture changes depending on the operating conditions of the cycle.

Nonuniform distribution, or maldistribution, occurs when parallel sections of the evaporator receive different mass fluxes, qualities, or both. Since the heat transfer coefficient (HTC) for two-phase refrigerant is orders of magnitude higher than that of vapor, any sections which experience dryout have much lower HTCs than other sections. In addition, due to vapor superheating, the temperature difference between dried-out sections and air is decreased. When these two effects of dryout are combined, the capacity and efficiency of the section drops significantly.

In applications where space and weight are important issues, such as in automobiles, heat exchangers with multiple parallel paths are used. As the number of paths increases, the size of the tubing decreases, and dryout occurs very quickly in sections with low liquid mass flow rates. For these conditions, maldistribution can affect the capacity and efficiency of the heat exchanger by a factor of 50%.

1.2 Literature Review

Refrigerant maldistribution is not a new problem, and studies have been conducted to determine its causes and effects for many years. Research exists for a wide variety of fluids, qualities, geometries, heat exchangers, and measurement techniques. The majority of recent studies concentrate on plate or serpentine heat exchangers, with a few FMT heat exchanger investigations. Relatively few studies include flow visualization of two-phase flows, and most are of air-water mixtures. The following is a chronological overview and description of published research on heat exchanger maldistribution.

Bajura and Jones (1976) studied the flow distribution of air in four types of manifolds. They found that the uniform flow distribution in the lateral paths is attained only when the headers act as infinite reservoirs, and they identified the most important parameters affecting flow distribution: manifold area ratio (total lateral tube area/inlet tube area), lateral flow resistance, header length/diameter ratio, diameter ratio between headers, and friction factor of the tube.

Bassiouny and Martin (1984) provided an analytical solution for flow distribution and total pressure drop in plate heat exchangers. They found that uniform and nonuniform flow distribution among the parallel conduits could be obtained depending on the ratio of the cross sectional areas of the intake and exhaust ducts. They also concluded that the uniform distribution could be obtained regardless of the number of plates and their shape by properly choosing this area ratio.

Asoh et al. (1991) observed the flow pattern of R113 two-phase flow in a manifold which separates into three vertically downward branches. Thermal loads were used to simulate a serpentine type evaporator. The flow pattern in the main pipe was set as either a slug or froth flow. They found that the flow pattern in branch pipes was not uniform, the liquid flow rate in the header greatly affected the flow distribution, and the slip flow model was more appropriate than the homogeneous model.

Rong et al. (1995) conducted an adiabatic experiment to study two-phase flow distribution in a stacked plate heat exchanger. Air/water two-phase flow was used in the experiment. They found that the flow distribution was highly nonuniform under most conditions and the vertical upward flow and the flow at low gas flow rates showed a better flow distribution. They also identified the most important parameters affecting flow distribution: flow pattern in the inlet tube (inlet flow rate and quality), flow channel orientation, and geometry of the channel inlet port.

Kariyasaki et al. (1995) observed the flow pattern of air/water two-phase flow in the manifold separating into three vertically upward adiabatic branches to simulate a serpentine type evaporator. The inlet flow pattern was set as a slug flow. They found that the flow pattern in the branch pipes was either slug or annular, and that the maldistribution decreased as the flow rate of the outlet manifold increased. The liquid distribution ratio increased and the gas distribution ratio decreased in the flow direction of the header when the flow rate of outlet manifold was small.

Watanabe et al. (1995) observed the flow distribution of R11 two-phase flow in a manifold which separates into four vertically upward branches. Thermal loads were used to simulate a serpentine type evaporator. They found that the flow pattern (mass flow rate and quality) at the header inlet dominated the flow distribution for adiabatic conditions. The pressure drop along the pass was found to affect the flow distribution when the heat load was applied, and a more uniform flow distribution was observed when the heat load was applied. They also found that T-junction data can be used to predict the flow distribution and pressure drop in a manifold.

Fei et al. (2002) observed the flow distribution of R134a two-phase flow in the inlet header of actual plate evaporators. They found that two-phase flow, especially a homogeneous two-phase flow with tiny droplets, showed a better flow distribution than the single-phase case. The introduction of baffles improves the two-phase flow distribution by obstructing the recirculation flow, although a large portion of the flow went in to the last branch in most conditions.

Zietlow et al. (2002) proposed a new method of measuring the liquid distribution in a microchannel heat exchanger manifold. Water and air were used, and distributed to a header with 20 parallel tubes, and the liquid flows to each tube were measured with load cells. The study was conducted at low pressures, and the method was validated by duplicating previous studies on water-air flow distribution.

Sa et al. (2003) investigated refrigerant maldistribution in flat multiport heat exchanger headers for two-phase R22 of 20% inlet vapor quality. Thermal imaging was used to visualize the thermal capacity distribution among the 32 microchannels in vertically upward orientation. Baffles were used to increase the number of passes and decrease the number of tubes in a header. The best flow distribution and performance was found to be with no baffles, opposing in-line flows to the inlet header, and two in-line outlets at the exit of the heat exchanger. They found that maldistribution can reduce heat exchanger capacity by up to 50%.

Cho and Cho (2004) studied the flow distribution of two-phase R22 in a round header with microchannel tubes. They evaluated the effects of header orientation, inlet quality, and inlet location. They found that horizontal headers with vertically upward flow provided better phase and mass distribution than vertical headers with horizontal flow, and the effect of inlet quality (0.1-0.3) on mass distribution was negligible. Increased inlet quality did result in a better phase distribution, especially for the last few paths. Cross-flow and parallel inlets provided better distributions than an in-line inlet.

Vist and Pettersen (2004) observed the two-phase flow distribution of both CO_2 and R134a in twelve header designs. They found that the best distribution was found for round tube manifolds, with vertically downward or upward flow depending on header diameter. They also found that for heat exchangers with 10 microchannels, the best liquid distributions were found for downward flow. However, a relatively effective distribution was obtained with an upward flow orientation by using a static mixer at the

inlet of the header. The tube pitches used in these microchannel heat exchangers were either 15 or 21 mm, and tube insertion depth was between 0.4 and 0.6 of the header diameter. The standard deviations of tube cooling capacity for the best R134a microchannel heat exchanger distributions were between 29-39% of the average. Flow visualization was performed for round tube manifolds only.

Hrnjak et al. (2004) evaluated the literature on two-phase distribution in evaporator headers, and provided a map of the best distribution ranges for round-tube heat exchangers. They found that the best conditions for round-tube evaporators are vertically downward flow, with approximately 33% vapor quality and 450 kg/m^{2}s mass flux. They found that conventional methods for obtaining good phase and mass distribution are limited to heat exchangers with fewer than 30 tubes in parallel.

The refrigerant flow distribution in multiple port heat exchangers which have headers and multiple tubes can be anticipated from the previous studies summarized above. However, most previous studies focus on flow distribution in plate or serpentine heat exchangers. Since the geometry of the multiple port heat exchangers is different from ones that have been studied previously, the two-phase flow distribution in multiple port heat exchangers needs to be studied. In addition, no study which performed visualization of microchannel headers was found in the literature search.

1.3 Objectives

The focus of this work is the construction of a test facility that quantitatively and qualitatively measures maldistribution in the inlet header of a flat multiport tube (FMT) heat exchanger. In order to fully understand the factors which govern maldistribution, the test facility should be based around a modular heat exchanger, and allow for visualization of the inlet header flow. The heat exchanger must allow for changes in tube pitch and number, to better gauge their effect on flow distribution. The location of the inlet to the header should be adjustable as well. The following quantities should be measured for each flow path of the heat exchanger: mass flow rate, pressure drop, quality, heat input, and temperature. Pressure drop should also be measured across the inlet header itself. The test facility should reflect the findings of previous studies in terms of optimal heat exchanger orientation, inlet location, and tube design. Lastly, the facility should use refrigerants as the working fluid.

The objective of this thesis is the construction of a test facility which meets all of the above design criteria. Specifically, the test facility should measure the influence of all of the following variables on maldistribution, while keeping all other parameters constant:

1. Refrigerant
2. Mass Flow Rate/Mass Flux
3. Tube Pitch
4. Tube Number
5. Heat Load
6. Inlet Location

2 Background

2.1 Refrigeration and Air-Conditioning

Refrigeration and air-conditioning systems play an important role in our everyday life. Air-conditioning systems exist in our offices, homes, personal automobiles, buses, airplanes and almost every closed environment that we deal with on daily basis. Refrigeration systems are used extensively in the food industry as well as many other industries such as gas separation, natural gas liquefaction, and ice production.

The most commonly used systems in air-conditioning and refrigeration industry are the vapor compression cycles. Vapor compression cycles have many complex variations, but a basic vapor compression cycle consists of four main components: compressor, condenser, expansion valve, and evaporator. The compressor is the only moving part of the system, and it compresses a refrigerant gas at low pressure to a higher pressure. This process is often assumed to be isentropic. The superheated vapor which exits the compressor then enters a heat exchanger called a condenser, where it is condensed and subcooled. The subcooled liquid refrigerant which exits the condenser is then expanded to a lower pressure with an expansion valve. This process is assumed to be isenthalpic, and normally results in a two-phase refrigerant flow into the next component, the evaporator. The evaporator provides the useful output of the cycle, cooling power, which is called the capacity. A vapor compression system's efficiency is measured by COP, or coefficient of performance, which is equal to the capacity divided by the power consumption.

2.2 Multiport Headers

In heat exchangers with many parallel paths, multiport headers are often used to distribute the inlet flow and collect the outlet flow from the different tube sections. Multiport headers can be constructed in a wide variety of geometries, both simple and complex. The simplest type of multiport headers is a cylindrical manifold with the heat exchanger tubes inserted into its cross section, in a series of T-junctions. Figure 1 is a drawing of such a manifold which was used by Vist (2004).

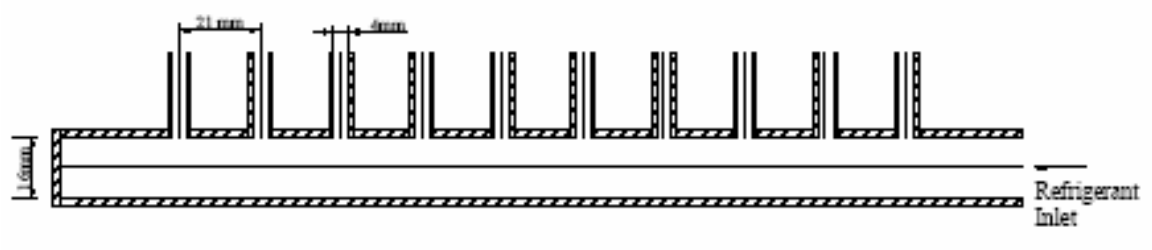

Figure 1 – Round Multiport Header with Round Tube Outlets, In-Line Inlet

The design shown above is easily adaptable to different tube shapes, inlet locations, number of tubes, and other geometric factors. Tube insertion into the multiport header is also common, though not shown in this drawing. Multiport headers and their heat exchanger tubes are typically assembled and then brazed in a furnace.

2.3 Microchannel Heat Exchangers

In applications where size and weight are important concerns, such as the automotive industry, compact heat exchangers are used. Microchannel heat exchangers are often used for these applications, because of their excellent capacity-to-volume characterstics. A microchannel is a flat multiport tube, with individual tube hydraulic diameters on the order of 1 millimeter. The advantage of this type of geometry is that the heat transfer

areas are very large relative to the mass flux. However, since pressure drop is also a concern, a large number of these microchannels must be used in parallel to distribute the total flow. Figure 2 is an image taken from Hrnjak (2004) of a microchannel heat exchanger used in a CO_2 system, which is able to withstand pressures up to 15 MPa.

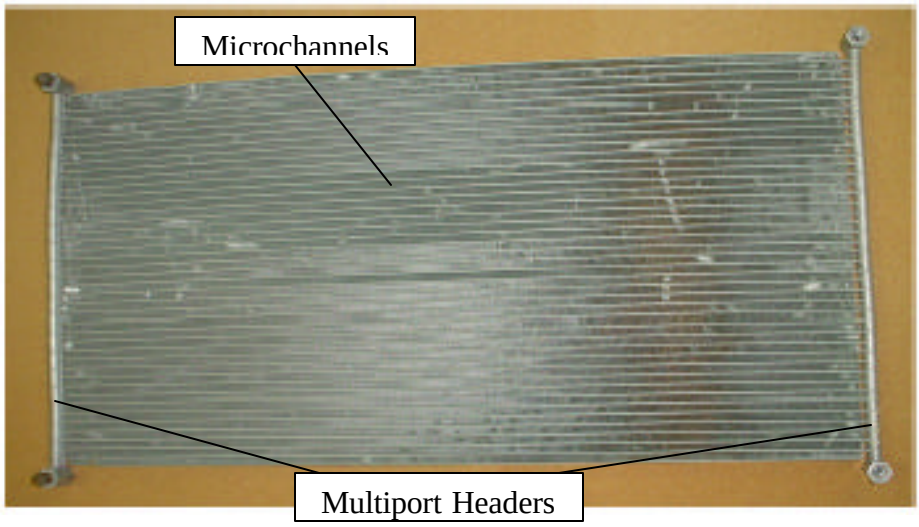

Figure 2 – Microchannel Heat Exchanger for CO_2 system

In most automobiles, microchannel heat exchangers are used as radiators and evaporators. Because of condensate drainage issues, automotive evaporators are normally installed with vertical headers and horizontal flow through the microchannels.

3 Experimental Setup and Test Procedure

3.1 Test Facility

In order to measure and observe two-phase maldistribution in multiport headers, a test facility was designed and created. The facility can be divided into two parts: a condensing unit, and an experimental system. Figure 3 shows the schematic of the overall test facility. The condensing unit is in the upper left corner of the schematic diagram, and its purpose is to provide cooling to the experimental system. The two systems are in a cascade arrangement, such that the condenser of the experimental system is the evaporator of the condensing unit cooling cycle.

The experimental cycle is a refrigerant loop containing the following thermodynamic components, in order: a gear pump, preheater/evaporator, and condenser. The evaporator is a microchannel heat exchanger with 30 parallel paths, and varying heat flux. The outlets of the heat exchanger are 10 round tubes, each of which contains the flow out of 3 microchannels. In order to measure mass flow rate and quality of the heat exchanger outlet tubes, the liquid and gas phases are separated for every outlet. Then, the 10 flows are combined, and the refrigerant is condensed and subcooled. This subcooled liquid is pushed through a magnetically-driven gear pump, and the cycle is repeated.

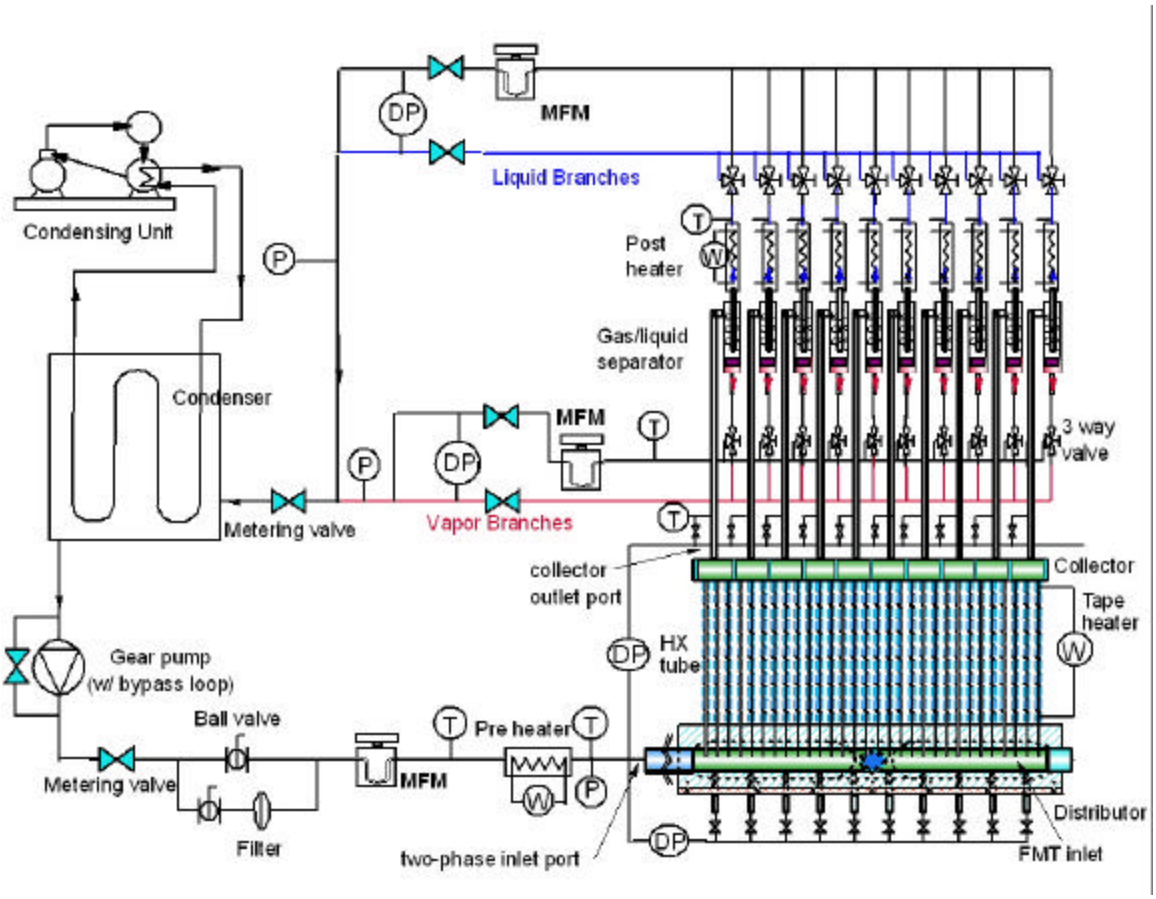

Figure 3 – Experimental Setup Schematic

Many sensors are used to monitor the system parameters, including mass flow meters (MFM), thermocouples (T), absolute (P) and differential (DP) pressure transducers, and wattmeters (W). The experimental setup will be described in detail beginning in Section 3.1.2.

3.1.1 Condensing Unit Cycle

3.1.1.1 Condensing Unit Cycle Design Criteria

A condensing unit is used in this work to provide cooling to the main experimental system. The selection of this condensing unit was done primarily by matching its capacity with that of the experimental system, which has two main components. The largest load is the 10 kW peak heat load across the test evaporator. In addition, 4 kW of latent heat is needed to reach the specified inlet quality of 30% at the most demanding conditions (R410A, 60 g/s, 5ºC evaporator outlet). In practice, this capacity estimation is generous, since the full 10 kW heat load is never maintained for a long period, and 7 to 8 kW is typical. The condensing unit which was chosen is an air-cooled, three horsepower R134a Copeland Semihermetic Condensing Unit, part number (P/N) CPDK-0300-TFC-001. The specifications for this condensing unit are shown in Table 1.

Table 1 – Condensing Unit Size and Performance Specifications, taken from Copeland's Website, https://www.customer-copeland-corp.com/jsp/Home.jsp

Mechanical

Unit Height (cm):	73.9
Unit Length (cm):	97.5
Unit Width (cm):	76.2
Condenser Type:	Air

Electrical

Max Fuse Size:	35
Min Circuit Ampacity:	25.4
Compressor:	2DF3-030E-TFC-100
Compressor LRA - Low:	
Compressor LRA - High:	102.0
Compressor LRA - Half Winding:	
Compressor RLA:	16.8
UL:	Listed
CSA:	Certified

Air - Cooled Unit Performance

Release Date:	09-Jan-2001	Return Gas Temp. (°C):	18.3
Compressor:	2DF3-030E-TFC-100 x 1	Subcooling (°K):	2.8
Performance No:	2880	Air Flow Rate (CMH):	6948.9

32.2°C Ambient Air Temperature

Evap. Temp. (°C)	Unit Capacity (Watts)
-17.8	5,550
-15.0	6,350
-12.2	7,150
-9.4	8,000
-6.7	8,950
-3.9	9,900
-1.1	10,900
1.7	12,000
4.4	13,150
7.2	14,350

As shown in Table 1, for 32.2ºC ambient temperature, the capacity of the condensing unit is 14.35 kW. This capacity is adequate to the experimental system's cooling needs.

3.1.1.2 Condensing Unit Cooling Cycle Schematic

Figure 4 is a schematic of the condensing unit cooling cycle and shows the directions of the refrigerant flows, as well as the measurement locations and types for the system. The condensing unit for this study consists of a compressor and a condenser. In order to make a complete vapor-compression cycle, at a minimum, an expansion device and an evaporator/heat exchanger are needed. In this study, these components are used, as well as a filter-drier to ensure the system is free of impurities, and a hot gas bypass to control the capacity of the system. Adding a hot gas bypass requires an additional metering valve. Pressure measurements were made using Setra gage pressure transducers, P/N C207, which range from 0-250 psig. Temperature measurements were done using T-type thermocouple wires that are attached to the outside of the system piping and insulated.

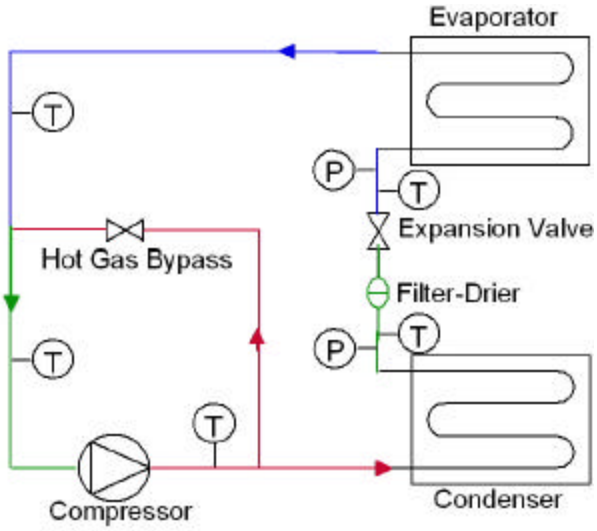

Figure 4 – Condensing Unit Cycle Diagram

3.1.1.3 Condensing Unit Cycle Components

The expansion device chosen for this work was a Swagelok expansion valve, P/N SS-12NRS-12, with a maximum C_V of about 1.8. A hot gas bypass was installed to lower capacity, with its own metering valve. The valve for the hot gas bypass is also produced by Swagelok: P/N SS-6NTRS-8. Both of the valves used for this cycle produce a linear change in C_V with respect to number of turns closed/opened.

A plate heat exchanger from Alfa Laval was used as the evaporator, P/N AC120-40EQ-S46. Its capacity was matched to that of the condensing unit.

A Catch-all brand filter-drier, P/N C-164, was obtained to keep the system clean. This type of filter-drier is rated for R134a systems of from 3-6 tons (10.5-21 kW).

A crankcase heater, Copeland P/N 918-0009-01, is also bolted to the compressor shell to prevent oil in the system from hardening in freezing temperatures. It provides 65 W of heating, and is powered with 208 volt, single phase power.

The system is insulated with black foam rubber of varying diameter, and secured in place with electrical tape.

3.1.1.4 Condensing Unit Cycle Installation Details

The condensing unit is located outdoors, next to the laboratory building. The unit is mounted on a waffled plastic pad, and an aluminum/steel mesh cover is used protect it from the elements. The unit is wired to an electrical disconnect, which provides up to 30

Amperes of 230 volt, 3 phase power. The condensing unit's safety devices (low oil and high pressure shutoffs) remained active, in the interest of preventing damage to the compressor. Figure 5 is an image of the condensing unit and electrical disconnect. Figure 6 is another view of the condensing unit and its cover.

Figure 5 – Condensing Unit and Electrical Disconnect

Figure 6 – Condensing Unit and Cover

The piping between the system components is nominally 5/8" outer diameter (OD) copper refrigeration tubing for the liquid lines, and 1-3/8" OD copper rigid tubing for the suction line. Near system components, however, changes in piping are necessary to accommodate the fitting types and sizes of the components. At the condensing unit liquid line (outlet of condenser), a 3/8" SAE flare connection is provided. The next component, the filter-drier, has 1/2" SAE flare connections. A combination of 5/8" tubing and brazed sweat connections is used to link these two components. At this point, the tubing is interrupted by a tee, where a pressure measurement is made. Next, the tubing is expanded to 3/4" OD at the expansion valve, which has compression fittings. Following the expansion valve, another tee is used for measuring pressure and also for

the system charging port. After the tee, the tubing runs to the plate heat exchanger. The plate heat exchanger's factory-provided connections are three 2-1/8" and one 7/8" OD sweat connections. Weld flanges are used to reduce the size of the larger connections to 3/4" OD, on which a stainless steel tube is welded. A 7/8" stainless steel pipe is welded directly to the smaller connection of the heat exchanger. After the smaller tubes are welded, compression fittings are used to make connections to outside piping. Figure 7 shows the plate heat exchanger after welding of the new connections.

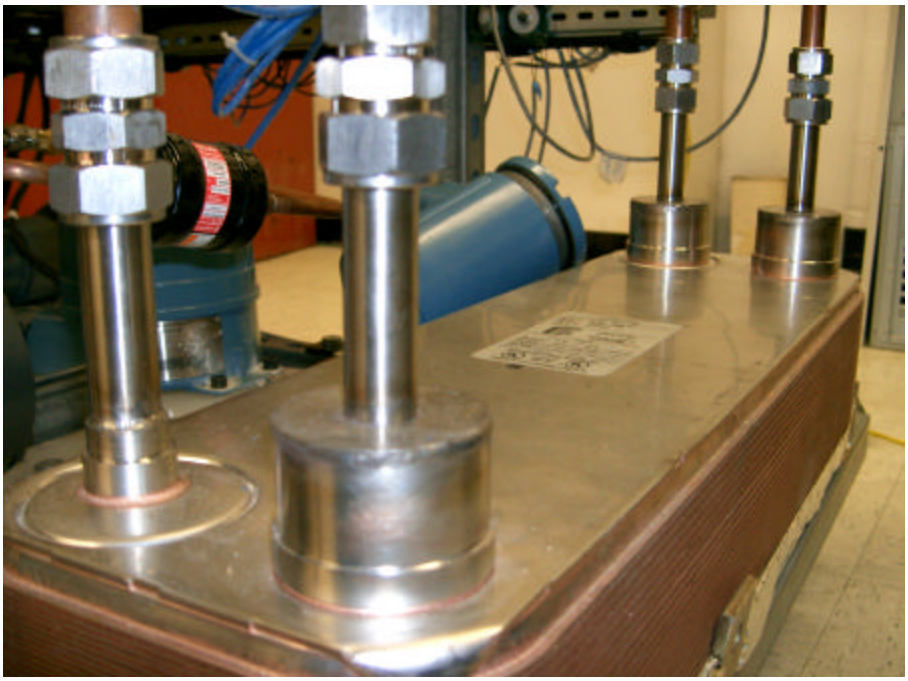

Figure 7 – Plate Heat Exchanger With Weld Flanges and Compression Fittings

The condensing unit cycle connects to the plate heat exchanger through two 3/4" OD compression fittings. As with other sections of piping, brazed sweat connections are used to change tube diameters as necessary. On the inlet side, 5/8" OD tube is changed to 3/4" OD near the plate heat exchanger. For the outlet, the 3/4" tube is expanded to 1-3/8" OD rigid copper tubing. This large tube is connected by brazing to the condensing unit,

which has a 1-3/8” OD sweat connection for the suction line. Both the 1-3/8” suction and 5/8” liquid lines pass through a single hole which is drilled through the wall of the building. Figure 8 is an image of part of the condensing unit cycle piping that shows most of the cycle components.

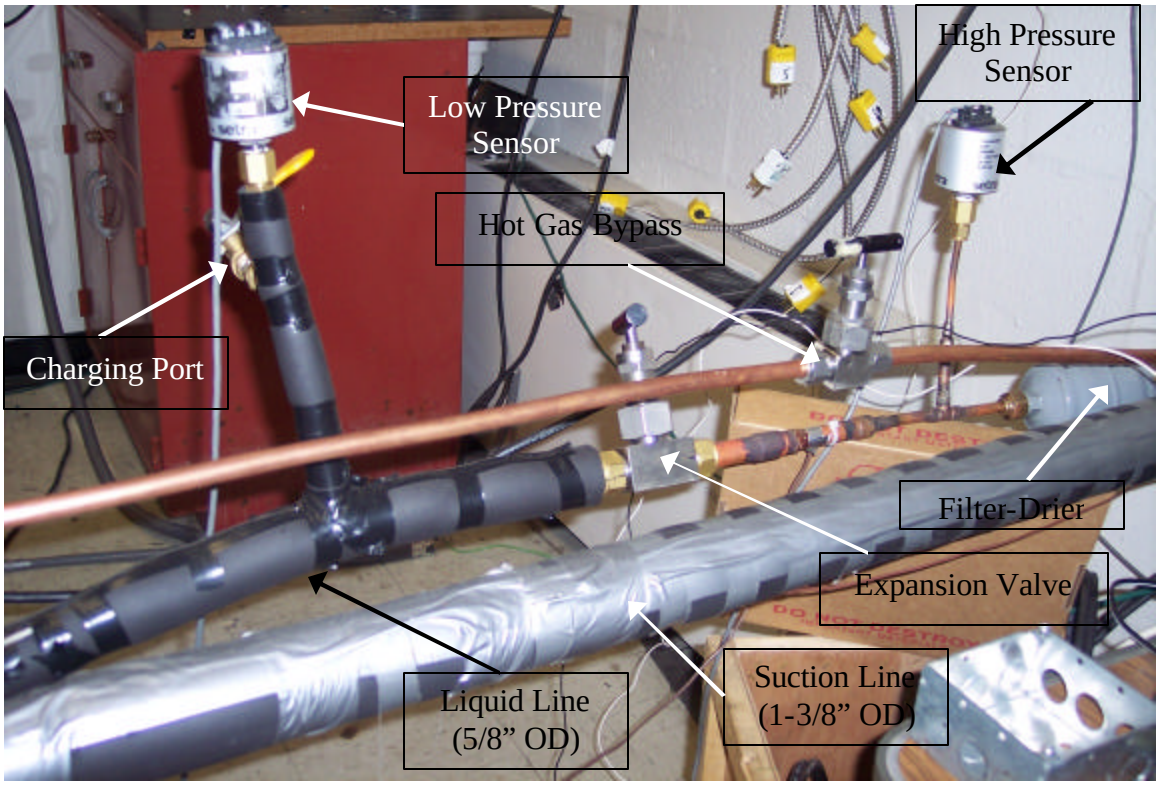

Figure 8 – Condensing Unit Cycle Piping and Components

3.1.2 Experimental System

3.1.2.1 System Schematic

The experimental system is designed to be a test stand for two-phase flow visualization. One important note is that although it is a refrigerant-charged system, the system is **not** a vapor-compression cycle. Any heat added to the experimental system during a cycle is removed in the condenser, which is cooled by the condensing unit system. Pressure

drops in the system are overcome with a gear pump. The full cycle diagram is given in Figure 3. Figure 9 is a simplified schematic of the experimental system's cycle, which shows the path of refrigerant flow through the system, using only one path of the test section as an example.

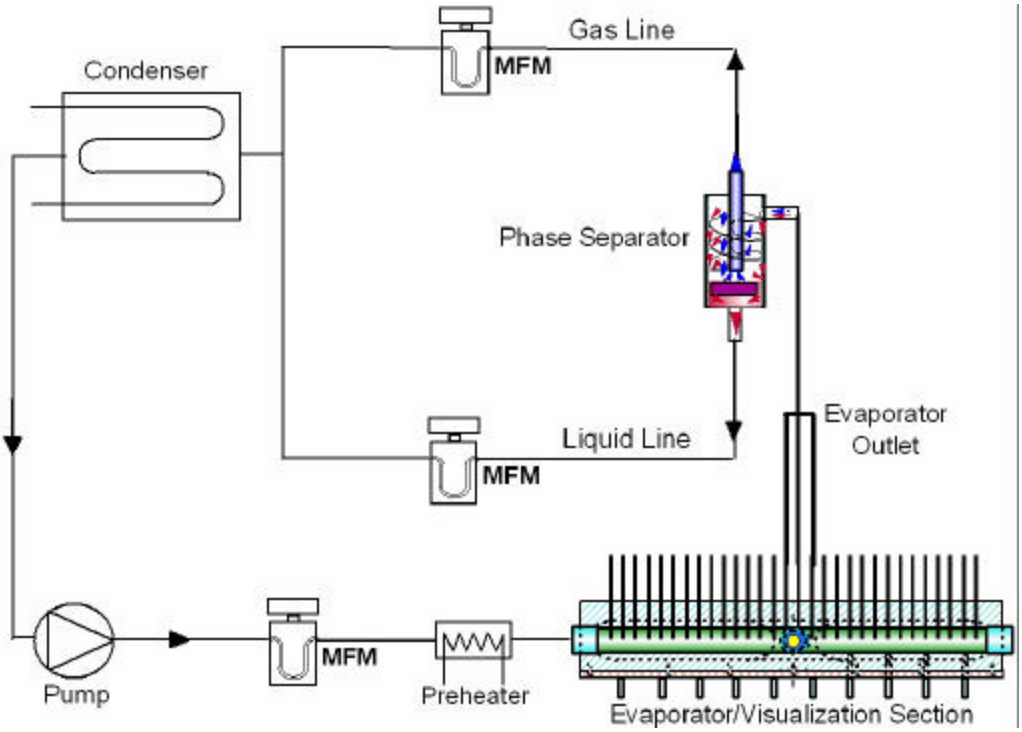

Figure 9 – Simplified Schematic of Experimental System

Starting in the bottom left portion of the figure, a liquid refrigerant flow is pumped to a mass flow meter (MFM), which measures the total mass flow through the system. Then, the flow passes through the preheater, which heats the liquid flow into a two-phase flow. Next, the flow enters the visualization section, which is the inlet to the evaporator. The main flow is distributed unevenly among 30 microchannels, and pushed through the heat exchanger. Electrical heating is used across the evaporator, in the form of heating tapes, which are used on each individual microchannel flow. For this schematic, only three of these microchannel flows are followed. After the refrigerant passes through the

microchannels, the flow enters a collector header, where the flows of 3 microchannels are combined. This flow, which is independent of all the other 27 microchannel flows, is then passed through a phase separator. The mass flow rates of both the liquid and the gas are then measured. Finally, the flows of all 30 microchannels recombine, and are passed through the condenser. The condenser removes all the heat from the cycle which was added by the preheater and evaporator, and the refrigerant begins another cycle. The majority of the system is insulated with black foam rubber of varying dimensions, which is secured in place with electrical tape. Heated regions of the system are protected with fiberglass insulation. The experimental system is located indoors, and its frame is constructed out of 1" steel Unistrut C-beams and 3/8" thick plastic sheet.

3.1.2.2 Visualization Section

3.1.2.2.1 Main Body

As stated above, the focus of this work is to create a test stand to visualize and measure two-phase flow distribution in an evaporator header. One of the biggest challenges of the study is to create a visualization section that allows for changes in test geometry, provides good visual access to the flow, and is leak-tight. In order to accomplish all of these goals, a modular design is used, based around a central piece, which is called the main body. The main body is designed to be machined out of rectangular stock, and have the following characteristics:

- A cavity in its center for the installation of a transparent acrylic header.
- Flat surfaces on the top and bottom along its length, which are used to bolt the microchannel heat exchangers and pressure taps to the chamber
- Cativities cut into the two sides where visualization is to occur, where flat gauge (noncircular) sight glasses are placed.

- Have o-ring seals on all surfaces and be completely leak-tight.
- Threaded NPT inlets at each end of the chamber, and also another NPT inlet located midway along the length of the chamber, on one of the sides with the glass pockets

Figure 10 is an image of the finished piece, with labels for critical features. The piece was machined out of a single piece of aluminum, with original dimensions of 5" x 2.5" x 18.5" (inches). Any metal with low thermal expansion and high strength can be used for this piece. Aluminum is used in the current work due to its high machinability, adequate strength, and low density/weight. Computer Numerical Control (CNC) was used to cut the o-ring grooves, and manual operation was used for all other work. The machining work was performed on a Bridgeport Milling machine on university premises, under the supervision of Howard Grossenbacher. An isometric perspective drawing of the piece is shown in Figure 11, next page. In Figure 11, the top, side, and end surfaces are labeled as well. The bottom surface is the surface which is located on the opposite side of the main body as the top surface.

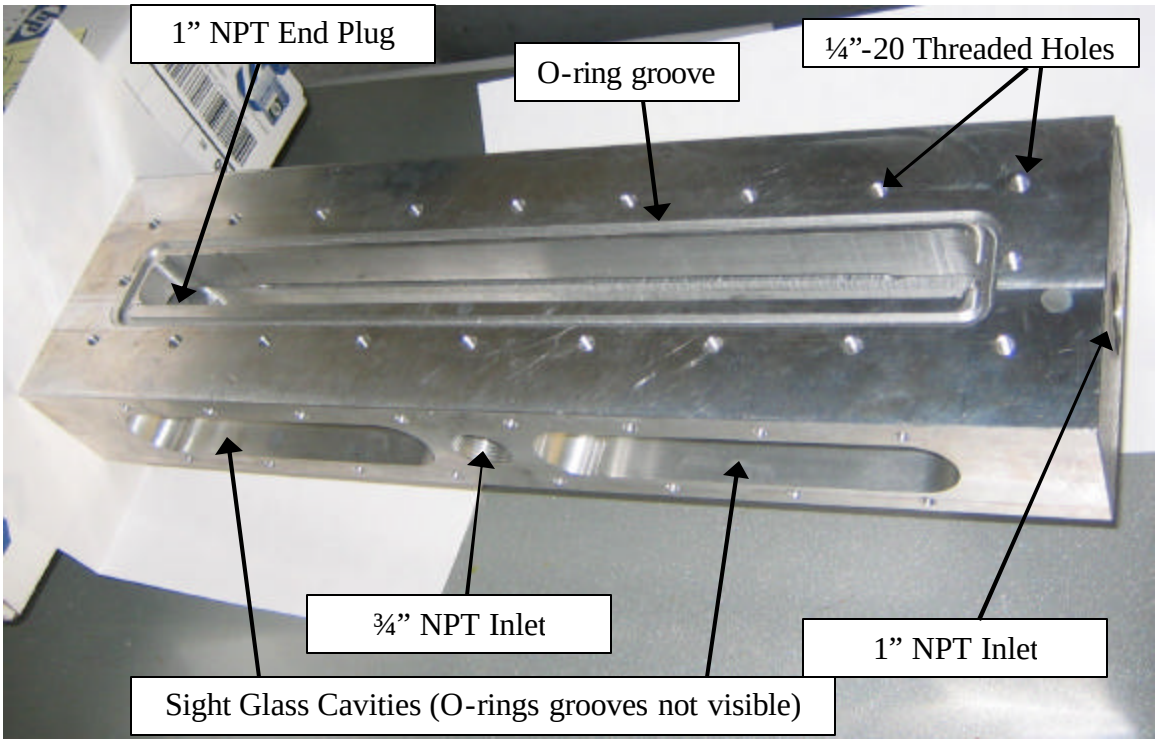

Figure 10 – Machined Main Body with Feature Details

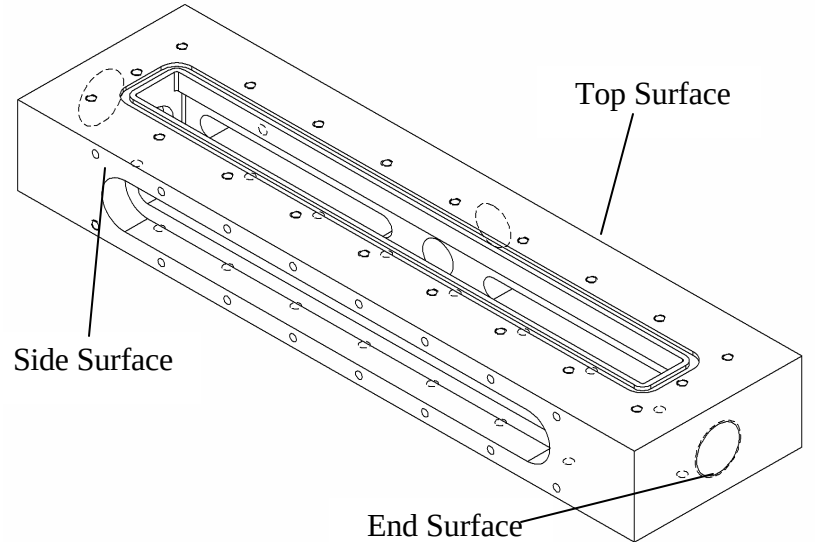

Figure 11 – Isometric Drawing of Main Body with Named Surfaces

The main body has many mating surfaces and connections. Figure 12 is an exploded view of the visualization section assembly which shows all the parts that attach to the main body.

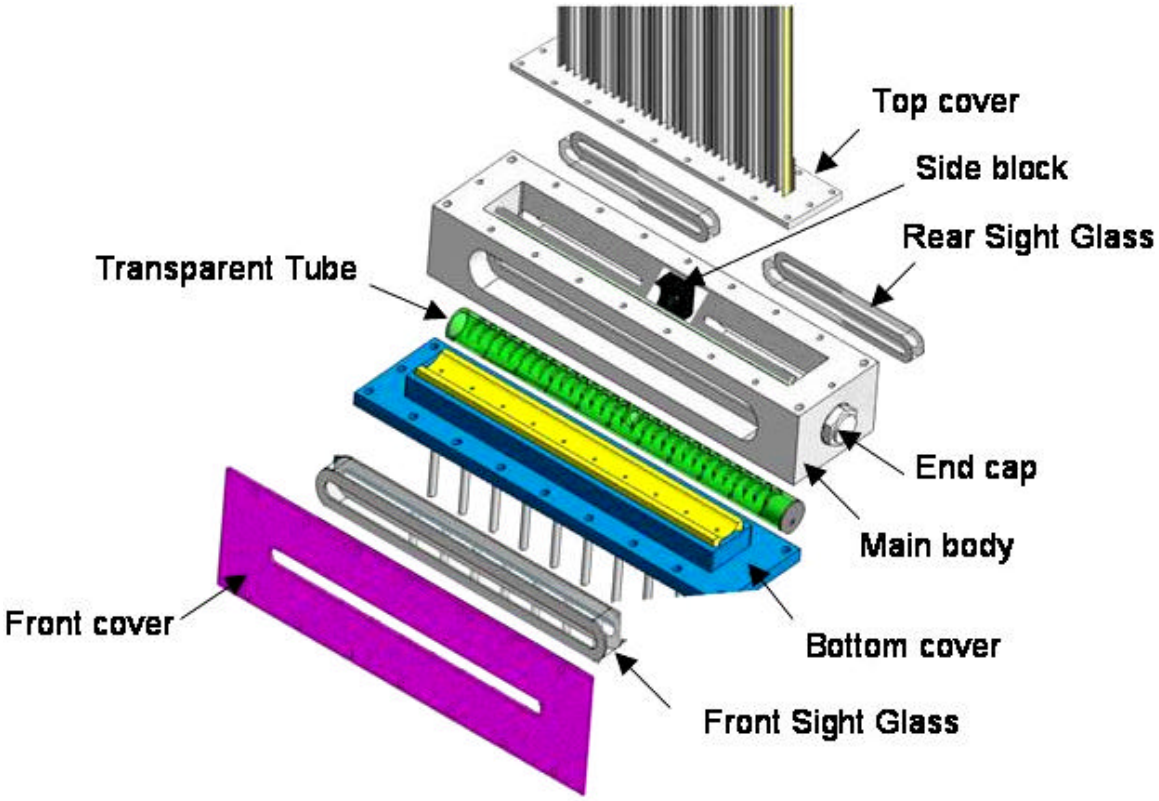

Figure 12 – Exploded View of Visualization Section Assembly

The top, side, and bottom surfaces of the visualization section are all sealed with o-rings. The o-rings and o-ring grooves for the assembly are *not* shown in this diagram. Neoprene is recommended as the o-ring material because of its proven compatibility with refrigerants and relatively low cost. All of the o-rings which are used in the experimental system are 70 durometer Neoprene. The o-ring grooves which are cut into the main body are based on the design methodology on www.efunda.com for o-rings on axial seals. SolidWorks and AutoCAD were used to determine arclengths and other dimensions for

size calculations. The specifications of the o-rings used in this system are detailed in Table 2.

Table 2 - O-ring Specifications and Standard Sizes

Surface Description	AS 568A Standard Size	Actual Sizes (in.)	
		Inner Diameter	Width
Top Surface	275	10.484 ± 0.055	0.139 ± 0.004
Bottom Surface	275	10.484 ± 0.055	0.139 ± 0.004
Small Sight Glass	242	3.859 ± 0.028	0.139 ± 0.004
Large Sight Glass	267	8.234 ± 0.050	0.139 ± 0.004

All of the o-ring grooves are cut to the same width and depth, only the length changes. The width of an o-ring groove is recommended to be 150% of the o-ring width, or in this case, about 0.2". The depth of the groove is 0.1", which corresponds to approximately 30% compression on the o-ring.

3.1.2.2.2 Transparent Tubes

At the heart of the visualization section is a transparent tube. This tube is machined out of clear Glycolized Polyethylene Terephthalate (PETG), and is obtainable through McMaster Carr, P/N 9245K35. This material was chosen for its optical access, relatively high maximum temperature (65ºC/150ºF), and machinability. The tubes are 1" OD, ¾" OD, and approximately 3 feet long. Figure 13 is the drawing used for machining these tubes.

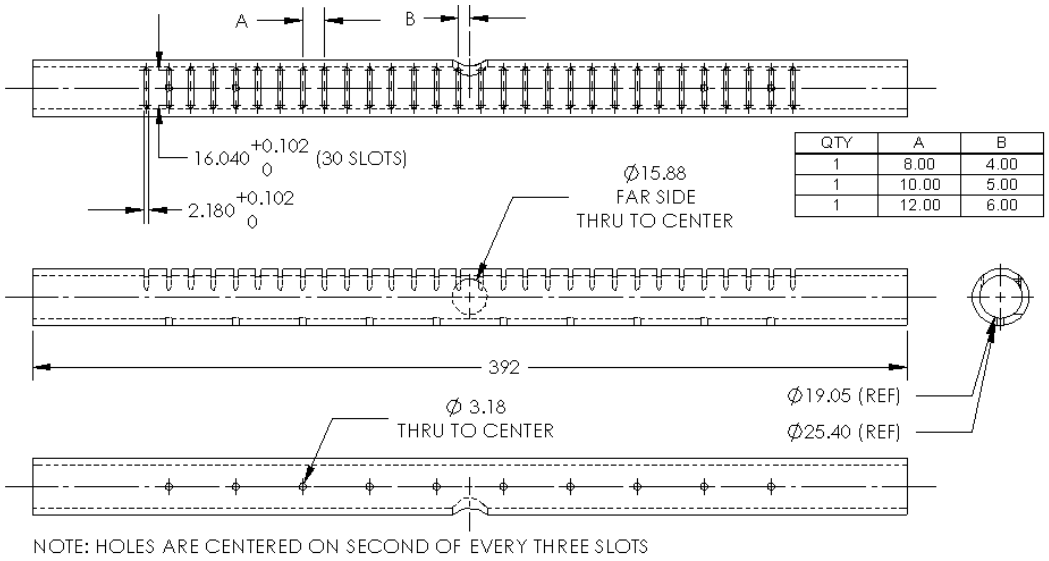

Figure 13 – Drawing of Transparent Tubes, with Dimensions in millimeters

As shown in Figure 13, the transparent tubes have 30 ports along the top of its length. These ports are sized to match the cross section of the microchannels used in this study. The spacing between these ports can be either 8, 10, or 12 mm, depending on the test condition. When the visualization section is fully assembled, the bottom edges of the microchannels are one radius inside the transparent tube. In addition to these microchannel ports, a 5/8" circular port is machined into the side of the tube halfway along its length. This port is used as the side inlet to the transparent tube. The end inlet is simply the end of the tube. The final manufacturing step is the drilling of 10 pressure taps (1/8" circular holes) into the lengthwise bottom of the tube as pressure taps. These pressure taps are located directly under the second of each group of three microchannel ports.

3.1.2.2.3 Dead Blocks

The transparent tube has 30 ports for microchannel insertion, each of which is always used during a given experiment. In order to block some of the microchannels, special blocks are inserted from either end of the transparent tube. These blocks, which are called dead blocks, are cut out of cylindrical plastic stock. Each block has two ends, one circular, and one semicircular. The circular end sits flush against the end of the transparent tube, and holds the block in place. The semicircular end blocks the refrigerant flow to the microchannels inside the transparent tube, by mating with the microchannels halfway into the tube. A drawing of a sample dead block is shown in Figure 14. The left side of the drawing is the end which sits flush against the transparent tube. A screw tap is present for installation purposes.

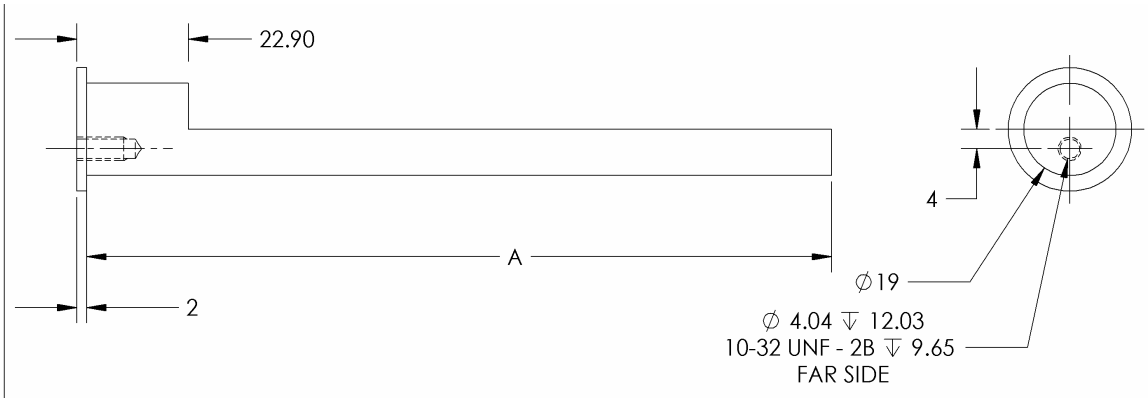

Figure 14 – Machining Drawing for Dead Block, with Dimensions in millimeters

3.1.2.2.4 Support Blocks

In addition to the transparent tube, several other plastic pieces are used inside the main aluminum body. These pieces, which are called support blocks, are used both to support the transparent tube, and also to provide an interface between flat surfaces and the curved

surface of the transparent tube. Figure 15 is an image of one of the transparent tubes used in this work, with these support/interface pieces.

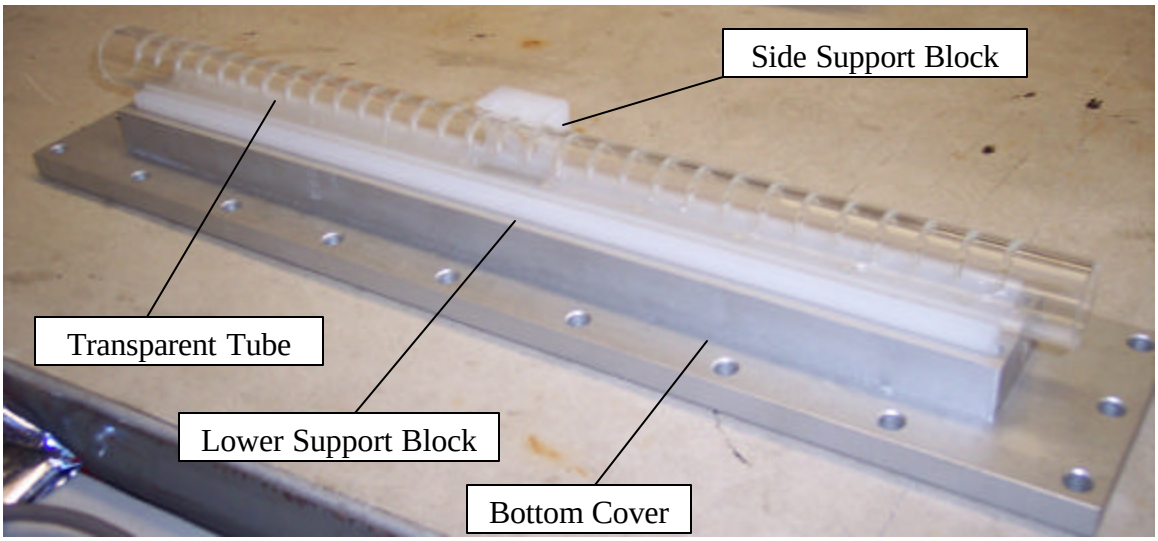

Figure 15 – 12 mm Pitch Transparent Tube, with Support Blocks and Bottom Cover

The figure shows a transparent tube resting on a long plastic support block, with a crescent shaped plastic block at the tube's side inlet. Both blocks are made of ultra high molecular weight polyethylene (UHMW), a material with excellent machinability and chemical resistances. The long support block sits between the transparent tube and the bottom cover to the main body, and is called the lower block. When the lower block is used in combination with the microchannels that are inserted into the transparent tube, the tube is fixed in place inside the main body. The lower block also has through-holes that are aligned with the pressure taps of the transparent tube. Since these pressure tap locations are different for each microchannel pitch, a total of three lower blocks are needed. Figure 16 is the machining drawing for the lower blocks.

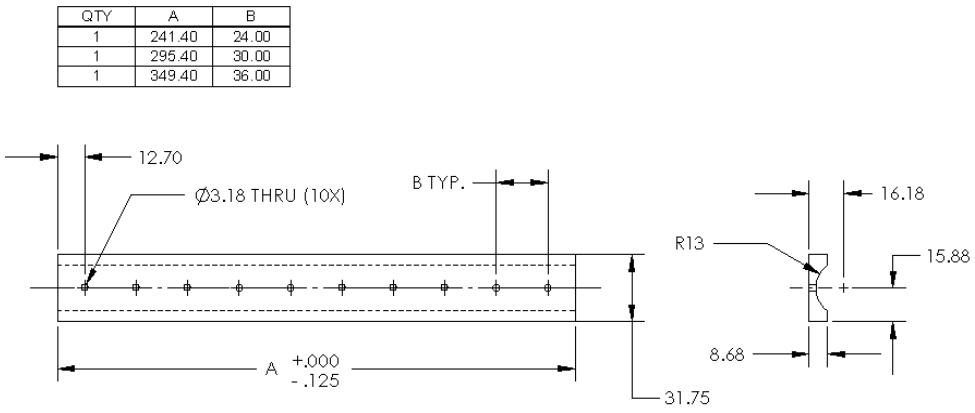

Figure 16 – Machining Drawing for Lower Blocks, with Dimensions in millimeters

The transparent tube's other support block are called a side block, and it is the interface between the tube and the main body's side inlet. Side blocks are curved on one side, flat on the other, and have a 5/8" diameter through-hole. The blocks are 1-1/8" in width, and about 1" in height. Although only one side block is used at a given time, several are necessary due to microchannel pitch differences. The reason for this is that some microchannels, impinge into the side block volume. Figure 17 is the machining drawing of the side blocks, showing each of a total of 3 geometries. In order to insert the current block in its place, a rectangular cut must be made in the lower block at the center of its length, on one side. This could be corrected in a future design.

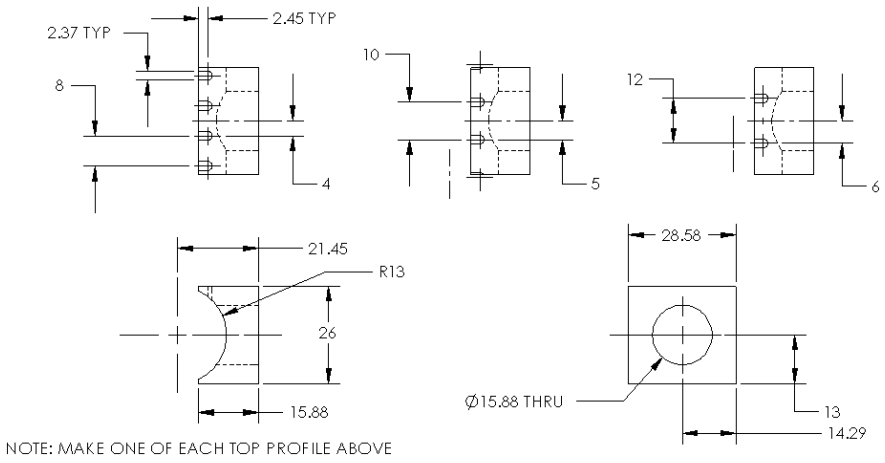

Figure 17 – Machining Drawing for Side Blocks, with Dimensions in millimeters

3.1.2.2.5 Bottom Covers

The bottom covers used in this work are aluminum blocks which are bolted to the bottom surface of the main body. Figure 12, on page 23, shows a given bottom cover's shape and position in the assembled visualization section. It is attached to the main body with twenty ¼"-20 threaded screws. Flat washers are also used to expand the contact area between the screws and the bottom cover. A neoprene o-ring is used to provide a leak-tight seal between the bottom cover and main body. The o-ring sits inside a machined groove on the main body's bottom surface. Figure 18 is the machining drawing for the bottom covers.

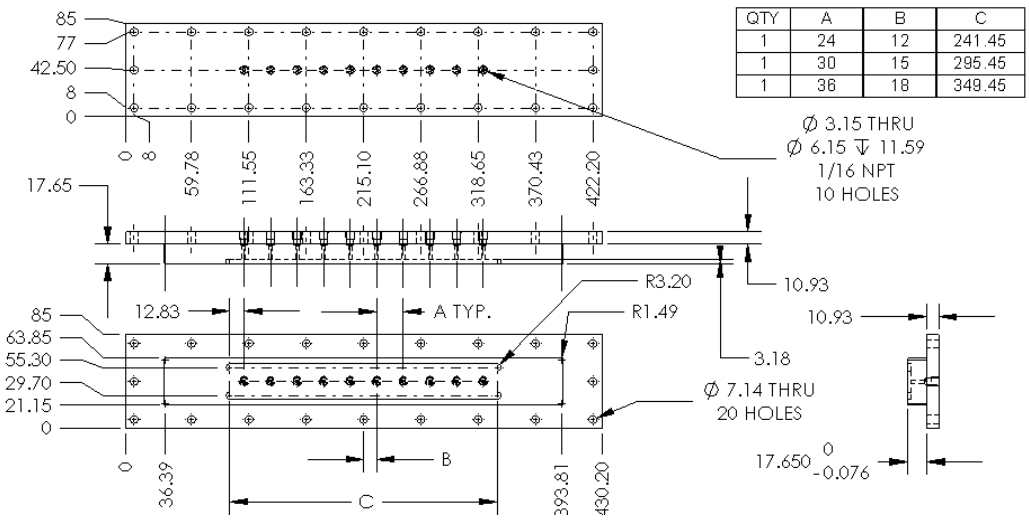

Figure 18 – Machining Drawing for Bottom Covers, with Dimensions in millimeters

The bottom covers serve two functions: supporting the lower block and transparent tube, and providing pipe connections for the pressure taps in the transparent tube. There are 3 bottom covers which are used in this work, corresponding to the 3 different microchannel pitches. Each bottom cover has 10 through-holes which align with the pressure taps in the lower support block. These through-holes are the same diameter as those of the lower block (1/8") at their interface on the top surface. On the bottom surface, the through holes are expanded into 1/16" NPT threaded connections (1/4" actual diameter). Finally, 1/8" depth cut is made in the top surface of the bottom cover. The shape of the recess is the same as that of the lower block for its respective microchannel pitch.

3.1.2.2.6 Top Covers

The top cover of the visualization section is also the base of the microchannel heat exchanger. It consists of two aluminum plates, one 1/8" thick, one 3/8" thick. Each of these plates has ports for thirty microchannels and twenty ¼"-20 screws to pass through. The screw pattern is identical to that of the bottom cover. As with other pieces, three

versions of the top covers are manufactured, one for each microchannel pitch. The thinner plate sits directly against the main body of the visualization section, and forms a seal with the neoprene o-ring that is set in a groove on the main body. When the screws are tightened on to top cover, the thinner plate is compressed between the main body below and the thicker plate above. The thicker plate's greater rigidity ensures that the thinner plate does not buckle or otherwise deform at the o-ring interface.

The reason for having a thinner plate is that brazing between the microchannels and the thicker plate is not feasible, since the thermal masses are too different. Thus, with a thinner plate, a better brazed connection can be formed with the microchannels. In practice, this method did not seal the interfaces completely, and epoxy is used between the thinner and thicker top cover to obtain a leak-tight visualization section. The epoxy used in this work is sold by Johnson Manufacturing Company, and is called Header Bond Epoxy, P/N 234-05. Applying the epoxy to this interface is made easier due to a recess which is present in the thick top cover, around the microchannel ports. Figure 19 is the machining drawing for the thick aluminum top covers. The thinner top cover has exactly the same width, length, and microchannel port sizes, but is only 1/8" thick.

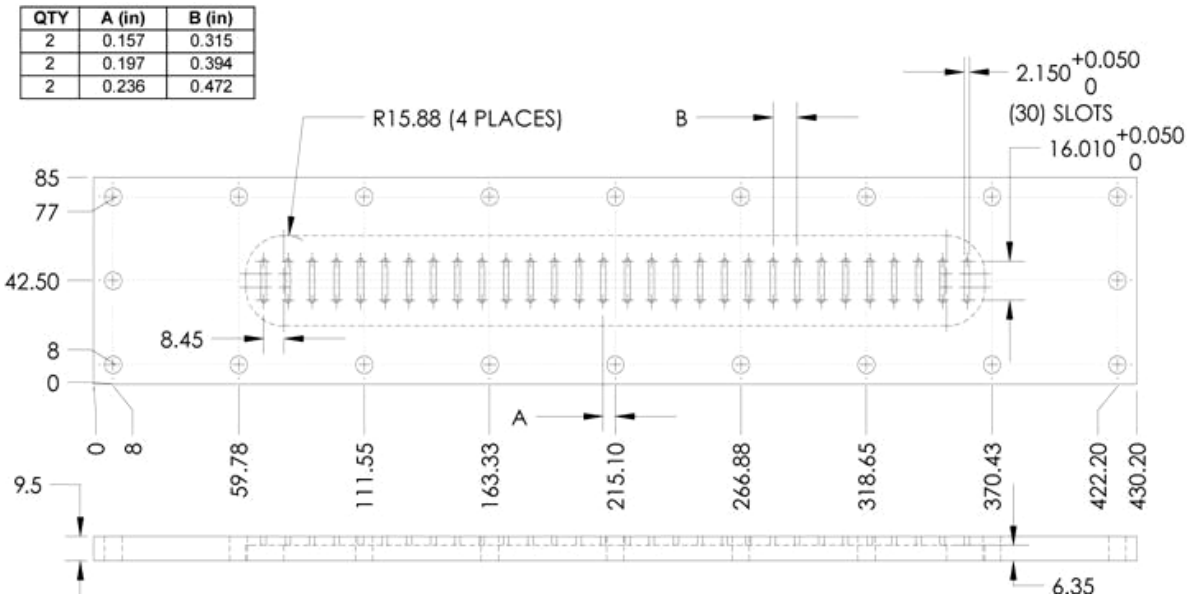

Figure 19 – Drawing of Thick Top Cover, with Dimensions in millimeters

3.1.2.2.7 Sight Glasses and Side Plates

The side surfaces of the main body each contain cavities – two small cavities on the side inlet surface, and one larger cavity on the opposite side of the main body. These cavities are sized to loosely hold transparent flat gauge pressure glass, to allow visual access to the transparent tube and the flow within. These pieces are called sight glasses, and their faces are rectangular in shape with semicircular ends. Figure 20 and Figure 21 are images of the sight glasses used in this work, which are sold by John C. Ernst Company. The P/N for the smaller sight glasses is 546-3, and the P/N for the large sight glass is 546-9.

Figure 20 – Small Sight Glass

Figure 21 – Large Sight Glass

The large and small sight glasses are identical in thickness, flatness, and width, but differ in length. The semicircular ends are the same dimensions for both sizes.

The cavities which hold the sight glasses have a width which is slightly larger than the width of the sight glasses, which are 1.325" wide. The semicircular ends of the sight glasses are also mirrored in the main body cavity. Similarly, the depth of the cavity in the main body is the same as the thickness of the sight glasses, 0.675". Then, the cavity is narrowed into a ¾" wide canal which is cut through to the center of the main body. The sight glass thus sits against a shelf of approximately ¼" width around the edge of the glass. An o-ring groove is cut into this shelf, and a neoprene o-ring is used between the glass and main body.

Since pressure must be applied to the sight glasses to obtain a good seal, more hardware is necessary for the side surfaces. For this work, sixteen ¼"-20 screw taps are made in each side surface of the main body, around the sight glass cavities. Next, face plates are bolted on to the main body, with viewports cut out in their centers for visual access.

These plates are called side plates, and they are made out of ¼" thick carbon steel plate. Fiber gaskets are used between the sight glasses and side plates to avoid damaging the glass surfaces. The viewports on the side plates are ¾" in diameter, and are bolted to the main body along the entire length of the sight glasses. The gaskets are made out of 1/16" thick C4401 sheet, which is a type of compressed fiber gasket produced by Klingersil. Figure 22 is an image of the large side plate and large sight glass assembled onto the main body. In the image, the brass fitting which is used in the ¾" NPT tap for the side inlet is visible, as are the bottom edges of the microchannels in the transparent tube.

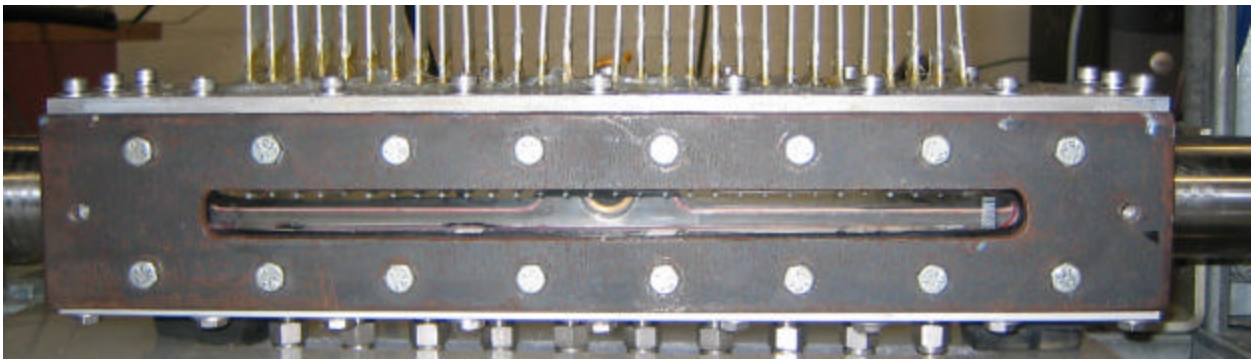

Figure 22 – Side Plate/Sight Glass Assembly on Main Body

3.1.2.3 Microchannel Heat Exchangers

The heat exchangers which are used as the evaporator for this work have headers at the outlet, and use the visualization section's transparent tube as the inlet header. The outlet header is called the collector, and the inlet header is called the distributor. Between the headers, 30 microchannels of 1 meter length are connected in parallel and constitute the main heat transfer surface. The microchannels are brazed to the top cover of the visualization section such that 1.19" of the microchannels extend through the plate. This dimension is essential to ensure that the microchannels extend one radius into the

transparent tube which is used as the inlet header. All brazing for this work was performed by Modine Manufacturing in Wisconsin. At the collector, groups of three microchannels are collected into 3/8" OD aluminum tubes, which are connected to the rest of the system with compression fittings. Internal blocks are brazed in place to prevent leakage from one outlet group to another. Figure 23 is a drawing of one of the microchannel heat exchangers in its assembled state. One important note is that the top cover is shown as one piece in Figure 23, but is in fact two pieces.

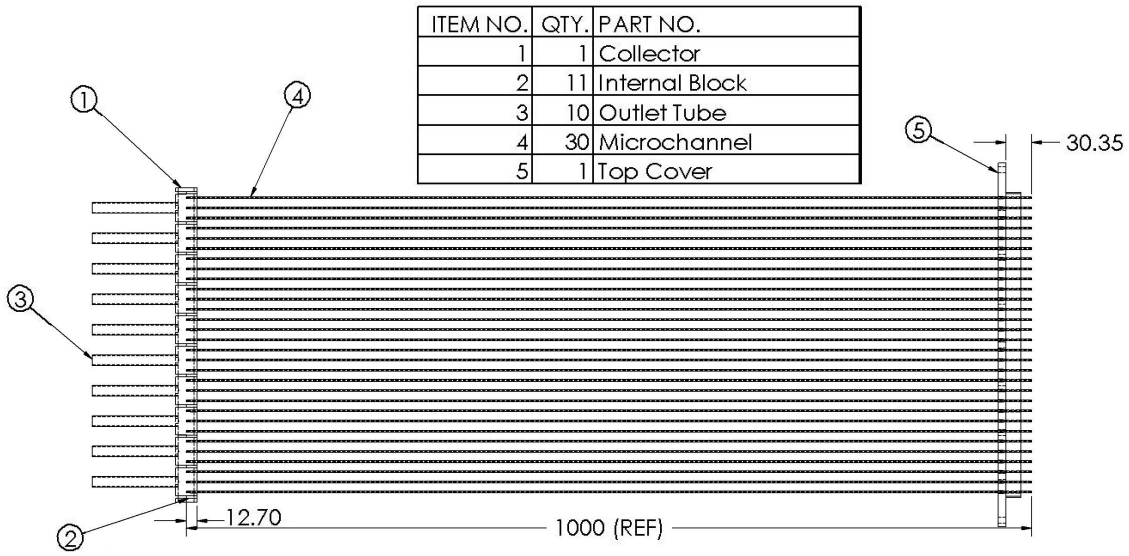

Figure 23 – Drawing of Microchannel Heat Exchanger Assembly, with Dimensions in millimeters

Figure 24 is a drawing of the cross-section of the microchannels used in this work. The microchannels each have six individual tubes with hydraulic diameters of about 1.69 mm.

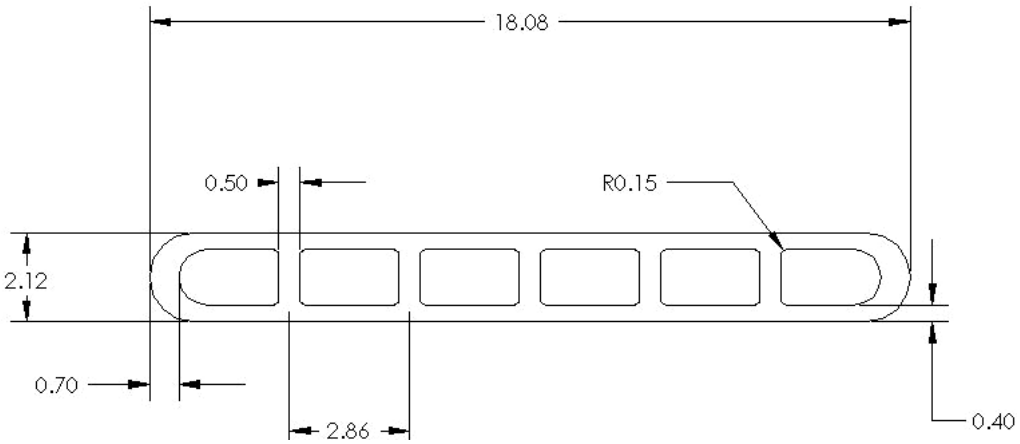

Figure 24 – Cross-Section of Microchannel, with dimensions in millimeters

Figure 25 is an image of one of the microchannel heat exchangers used in this work, prior to the application of epoxy between the top covers.

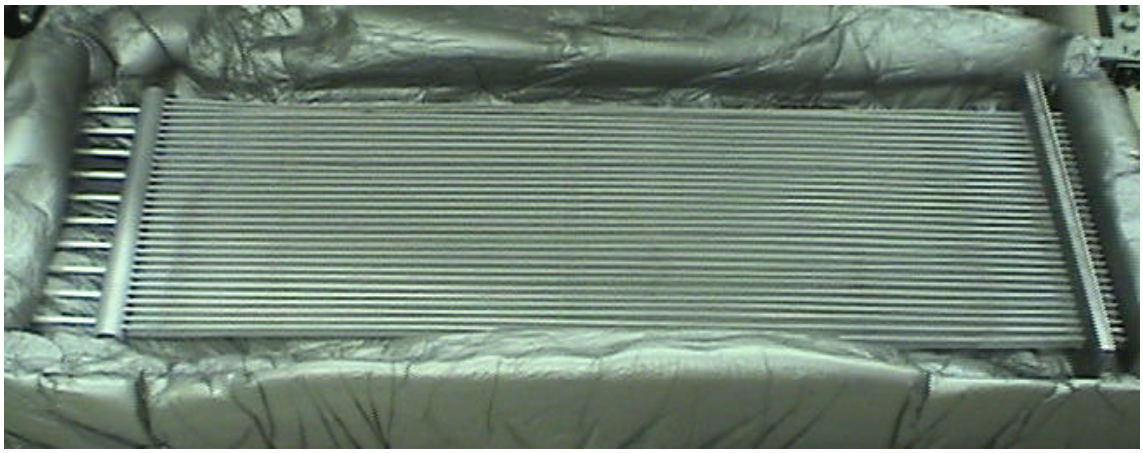

Figure 25 – Microchannel Heat Exchanger, 10 mm pitch, without epoxy

The collector tubes shown on the left side of Figure 25 are the location of the pressure measurement for pressure drop across the microchannel heat exchanger. A tubing manifold is attached to the outlet tubes, with shutoff valves such that any collector tube's pressure can be measured individually. The shutoff valves are brass ball valves which are produced by McMaster Carr, P/N 47865K21, with 1/4" NPT connections. Figure 26

is an image of the manifold and valves which comprise the differential pressure lines, as they are installed in the experimental system.

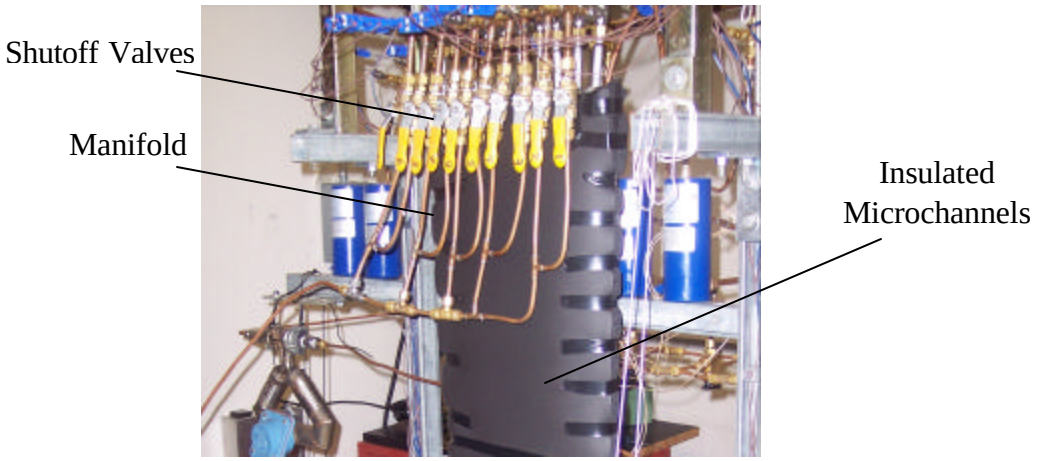

Figure 26 - Microchannel Heat Exchanger Differential Pressure Manifold

3.1.2.4 Heating Tapes

The test conditions for this work demand that equal heating be applied to each microchannel in the microchannel heat exchanger, up to a maximum of 10 kW for the entire heat exchanger. Heavy insulated heating tapes from HTS/Amptek, P/N AWH-051-060D, are used to meet this requirement. The tapes are 6' long, with electrical leads on one end, and pairs of woven strings on each end for tying the tapes to another structure. Each heating tape is roughly twice as long as the exposed length of the heat exchanger, and so the tapes cannot simply be attached to one side of a microchannel. Instead, a tape is laid flush against both sides of a given microchannel, and the tape is bent after 3' of length. Once aligned, the heating tapes are tied to the collector header of the heat exchanger by using the woven strings. Then, once the heating tapes are aligned with the microchannels, the microchannel-heating tape assembly is wrapped in thin tinned copper

wire (AWG 26) in a spiral to ensure good thermal contact. Figure 27 is an image of the microchannel heat exchanger after the heating tapes are installed.

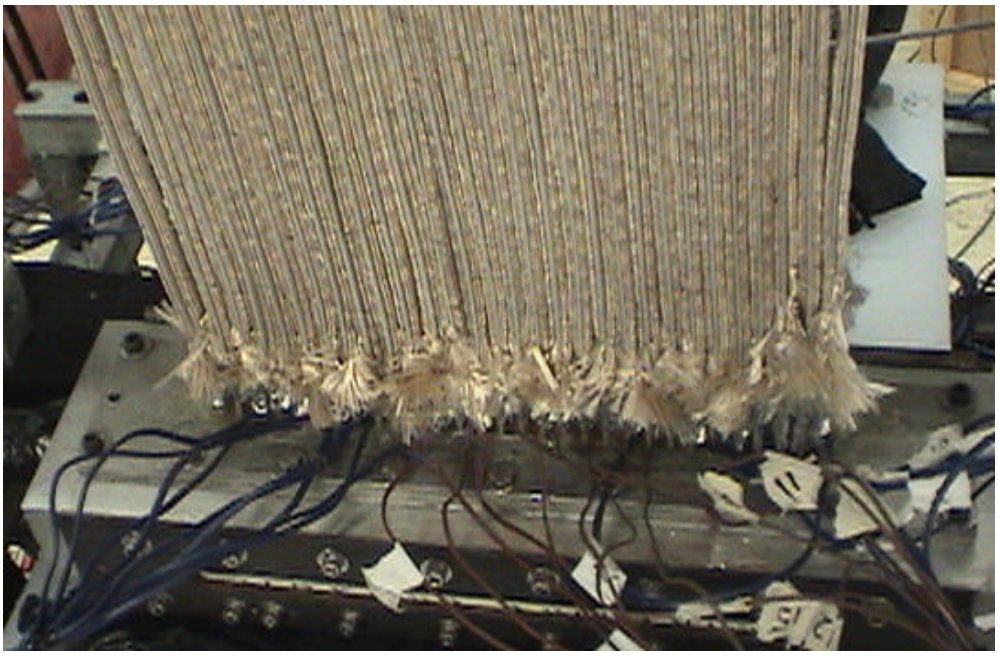

Figure 27 – Microchannel Heat Exchanger/Heating Tape Assembly

In addition to showing the appearance of the microchannel heat exchanger with heating tapes, Figure 27 also shows the assembled visualization section and many thermocouple wires. The thermocouples, which are discussed in Section 3.2.4 – Temperature Measurements are used to measure the temperature of the microchannels near the top covers/epoxy. The main purpose of these thermocouples is to prevent melting of the epoxy or microchannels.

The electrical characteristics of the tape heaters are as follows: each tape has a resistance of approximately 30 ohms, draws 3.9 amperes of 120 VAC, and provides 468 W of heating to an individual microchannel. The total heating power provided by all the heating tapes is 14.3 kW, although this number shrinks to 11.2 kW and 8.4 kW when the

number of microchannels used are 24 and 18, respectively. The tape heaters are powered by six building circuits, five of which supply 20 amperes, and one which supplies 30 amperes. Overall heat exchanger capacity is controlled by changing the fractional on-time for the heating tapes. The capacity control and wiring schematics for the heaters are discussed in Section 3.2.8 – Heater Controls.

3.1.2.5 Phase Separators

Ten 3/8" OD aluminum tubes serve as the outlets to the microchannel heat exchanger assembly. These aluminum tubes, called collector tubes, are connected to copper refrigeration tubing of the same size by using compression-type union fittings. These copper tubes carry refrigerant flows which are either two-phase or superheated vapor. If the flows are two-phase, the phases must be separated before any mass flow measurements can be performed. Each flow must also be kept independent of the other nine collector tube outlets, so a total of ten phase separators are needed.

The phase separators used in this work are helical separators from Henry Technologies, P/N S-5180. These separators are cylindrical, with 2.5" diameter and 6.38" height. Each cylinder has an inlet, a gas outlet, a liquid outlet, and an oil drain which is plugged for this work. The inlet and gas outlet are both ¼" OD sweat connections, the liquid outlet is a 3/8" flare connection, and the oil drain is a 1/8" NPT connection.

Although they are technically oil separators, the mechanism for phase separation is applicable to any two fluids with very different densities. The separators are cylinders, and the flow into the cylinder is forced into a spiral flow, with very high centrifugal

force. This forces the denser liquid to the walls of the cylinder, and gas collects in the center. Henry Technologies claims over 99% separation efficiency for inlet vapor fractions above 70%. Figure 28 is an image of a separator like the ones used in this work.

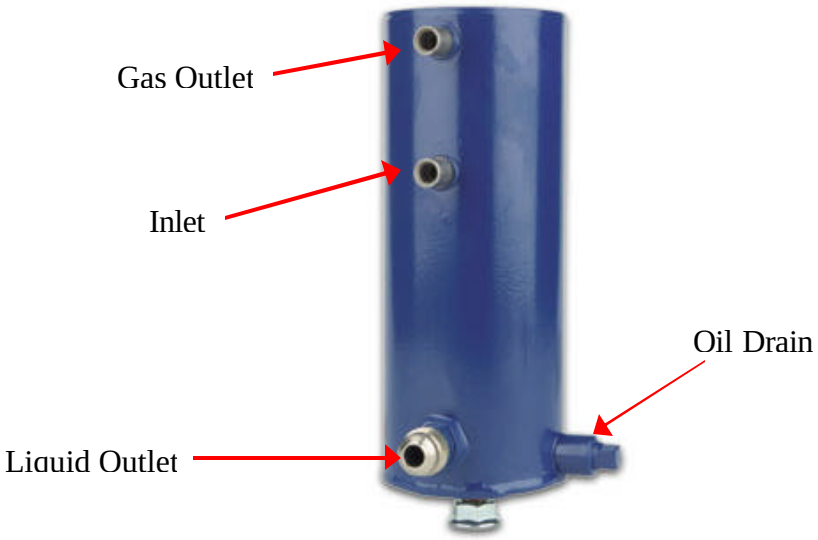

Figure 28 – Helical Phase Separator from Henry Technologies

In the experimental system, the collector tubes are reduced from 3/8" to ¼" OD copper through sweat connections to fit the separator inlet connection. The gas tubes are similarly expanded to 3/8" OD from the 1/4" separator gas outlets. The liquid lines are reduced from 3/8" OD at the separator liquid outlets to 1/4" OD tubing. Figure 29 is an image of the system before connections to the separator inlet are made, and after liquid and gas branches are installed. The gas outlet flows vertically upward, and the liquid outlet flows downward. This geometry prevents phase mixing by buoyancy or gravity effects.

Figure 29 – Sample Phase Separator Outlets

Figure 29, previous page, also shows heating tapes wrapped around the gas line. These tapes are similar to those used on the microchannel heat exchanger, and are called postheaters. Each postheater provides 106 W of heat when connected to a 120 VAC power supply, and is 2 feet long. The tapes are manufactured by Amptek, and are P/N AWM-051-020D. The purpose of the tapes is to superheat the exiting vapor from the phase separators, and evaporate any liquid which is in the flow.

3.1.2.6 Liquid/Gas Branches

The liquid and gas outlets of each phase separator are connected to three-way valves. Each liquid outlet's valve is part of a manifold which connects all ten separator liquid outlets to one of two paths: the main liquid flow, or the measured liquid flow. The same is true for the gas outlets. Generally, nine of the ten separators' liquid outlets are routed to the main flow, and one separator's liquid outlet flow goes through the measured path. Any of the ten flows can be redirected to the other path at any time by changing the setting of its respective three-way valve. Both flow paths are constructed of ¼" OD copper tubing, and all connections are made with compression fittings. The measured

liquid flow is termed as such because it is passed through a mass flow meter. Also, a sight glass is placed before the mass flow meter to ensure that single phase flow is entering the sensor. The mass flow meters used for the liquid and gas lines are MicroMotion ELITE Coriolis-type mass flow meters. They are discussed in detail in Section 3.2.1 – Mass Flow Rate Measurements. After the flow rate is measured, it passes through a needle valve. Then, an absolute pressure measurement is made, and finally a differential pressure measurement is made between the main flow and the measured flow. The measured flow also passes through a needle valve before the differential pressure measurement is made. At this point, the measured liquid flow is merged with the main liquid flow. The needle valves used for metering the flow are made of brass, have 1/4" NPT connections, and are sold by McMaster Carr, P/N 4995K13.

A duplicate schematic is used for the gas outlets to enable the measurement of any one of the ten separator gas outlets. A second set of sensors is used for pressure and mass flow rate measurements like those performed on the liquid flows. The main difference between the liquid and gas flows is the size of the tubing. Because gas flows experience greater pressure drops than liquid flows for the same mass flux and cross-section area, the tubing must be larger for the gas flows. Thus, the measured gas path is constructed with 3/8" OD copper tubing, and the main flow is passed through 3/4" OD copper tubing. The needle valves used in the gas lines are also sold by McMaster Carr, with 3/8" and 3/4" NPT connections for the measured and main gas lines, respectively. The part numbers for the brass valves are 4995K15 and 4995K19. The measured gas path connections are generally compression fittings, and the main gas path connections are mostly sweat

fittings. Figure 30 is an image of the manifolds as constructed in the experimental system. The tubing to the phase separators from the microchannel heat exchanger is not shown in the figure.

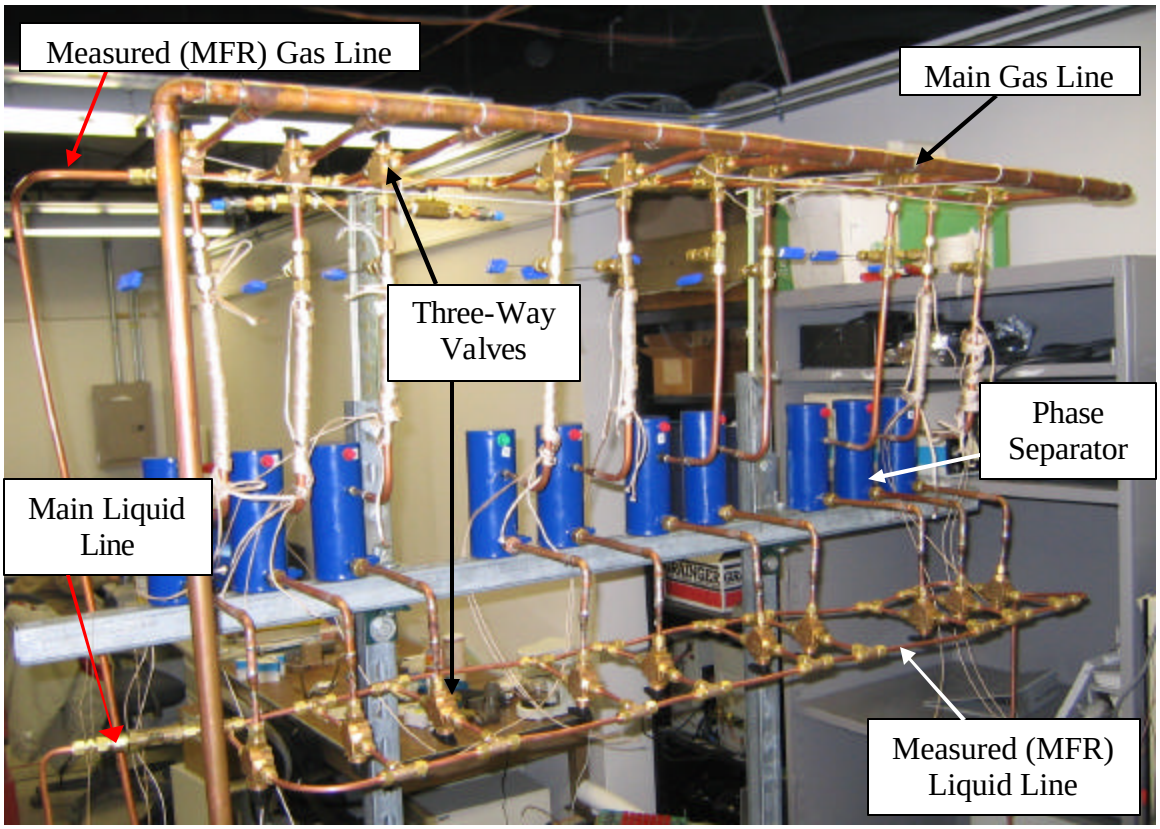

Figure 30 – Liquid and Gas Branch Manifolds in Experimental System

Figure 31 is an image of the intersection of the measured and main liquid lines. The junction of the measured and main gas lines is constructed in the same way. Once the flows from the main line and measured line are combined for both the liquid and the gas flows, the 1/4" OD liquid tubing is expanded with sweat connections to match the 3/4" OD gas line. The liquid line has two vertical u-bends prior to intersecting the gas line which prevent vapor from entering the liquid line due to buoyancy effects. Finally, the gas and liquid flows are merged into a single 3/4" OD tube flow. Figure 32 and Figure

33 are images of the sight glasses which are placed before the mass flow meters in the liquid and gas lines.

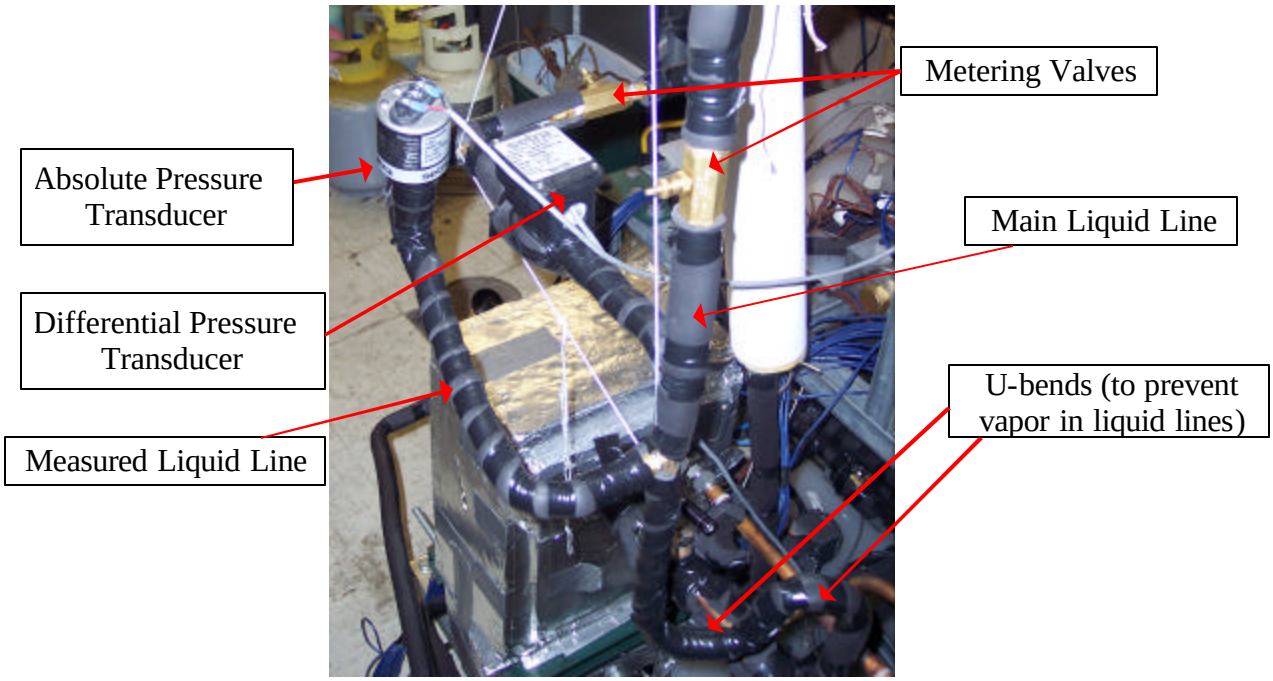

Figure 31 – Intersection of Measured and Main Liquid Lines

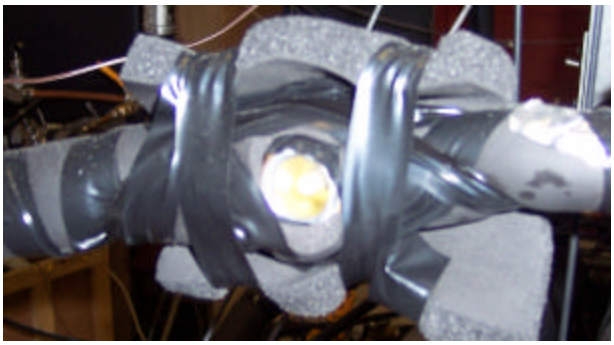

Figure 32 – Liquid Line Sight Glass with Moisture Indicator

Figure 33 – Gas Line Sight Glass with Moisture Indicator

3.1.2.7 Cascade Heat Exchanger

Once the liquid and gas flows are merged, the combined flow is immediately connected to a heat exchanger which is shared by the condensing unit and experimental cycles. This is called the cascade heat exchanger, and it is described in 3.1.1.3 – Condensing Unit Cycle Components. The function of the heat exchanger is to condense and subcool the refrigerant flow of the experimental cycle. The heat exchanger is mounted in an upright position, such that the entering flow on the experimental system side flows to the outlet by gravity. This orientation is also used to ensure that only subcooled liquid flows out of the heat exchanger during system operation. The heat exchanger has of 3/4" compression fittings at its inlet and 7/8" compression fittings at the outlet. The outlet piping is reduced to 3/8" OD with sweat fittings.

3.1.2.8 Gear Pump

The subcooled liquid refrigerant which exits the cascade heat exchanger in the experimental cycle is connected to a gear pump. This gear pump is the driving force of the experimental system, and it is designed to be able to overcome all pressure drops in the cycle. The pump must also be capable of producing a mass flow rate of at least 60 grams per second. Preliminary calculations indicated that at peak mass and heat input, the total pressure drop in the system would be equal to or less than 100 kPa. Other design considerations are that the flow be steady with respect to time (not intermittent or pulsed), and that the pump be oil-free. An external gear pump meets all of the design requirements, and the model used in this study is a Series 200 Micropump, P/N GB-P35PVSKP4. The pump is oil-less, and is magnetically driven by a 1/2 horsepower, 208

volt single phase, 3450 RPM AC motor. The pump is installed at the lowest point in the system to prevent cavitation (bubble) damage or failures. The inlet and outlet of the pump are both 1/4" NPT connections. Figure 34 is a performance graph of the gear pump used in this work. The figure is a plot of volumetric flow rate versus differential pressure for a fluid with 1 centipoise viscosity, which is a reasonable approximation of a liquid refrigerant flow.

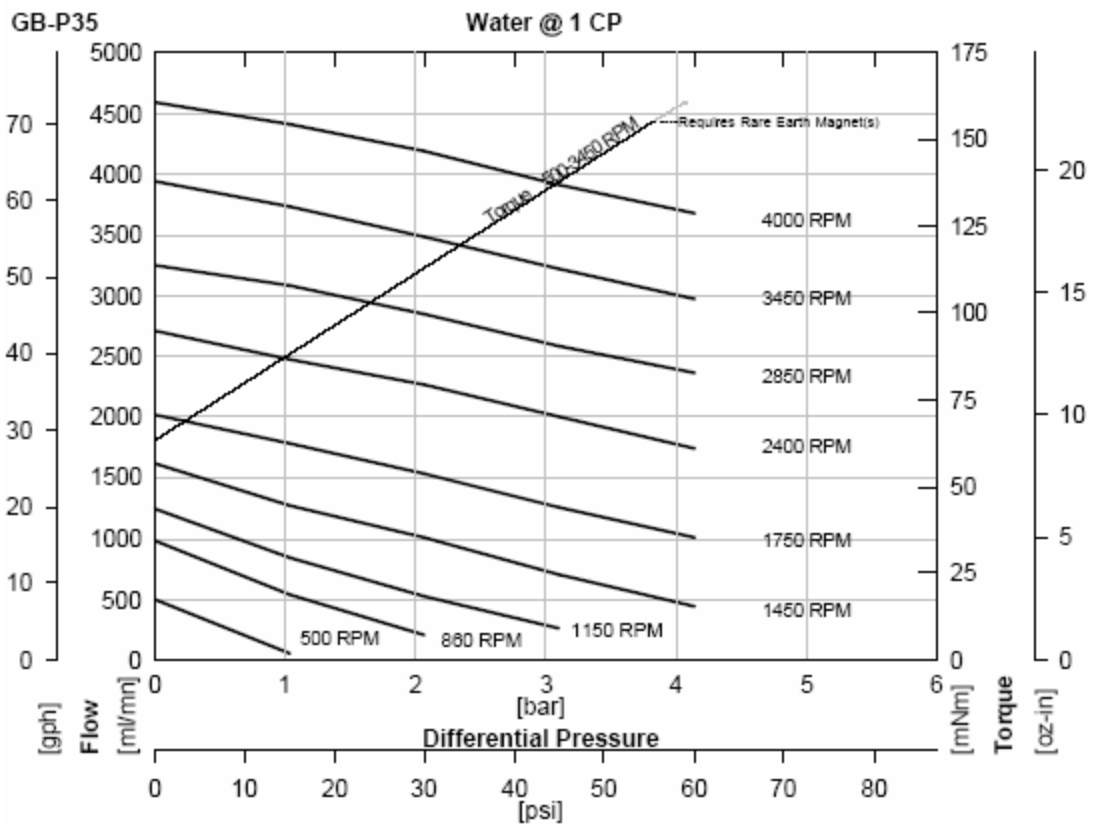

Figure 34 – Performance Graph of Gear Pump, 500-4000 RPM, taken from http://www.micropump.com/products/pumps/gear/series200.asp

The maximum differential pressure is 60 psi, or approximately 413 kPa. Mass flow rate specifications are obtained from the graph by multiplying the volumetric flow rate by the liquid density of the refrigerant. For the conditions in this work, the maximum mass flow rate is approximately 80 grams per second. Since these specifications exceed the

requirements of the cycle, it is necessary to use extra controls to lower the mass flow rate and pressure increase generated by the pump. In this installation, a bypass loop with a metering valve is used to regulate the mass flow rate, and a metering valve is also placed before the cascade heat exchanger to regulate the pressure in the system. The bypass loop is constructed with 3/8" OD tubing, and uses a needle valve identical to the valve in the gas measuring line. The in-line metering valve before the cascade heat exchanger is produced by Swagelok, P/N SS-18RS12. Figure 35 is an image of the AC motor/gear pump assembly in the system, with its bypass valve. The in-line metering valve is not visible in this image.

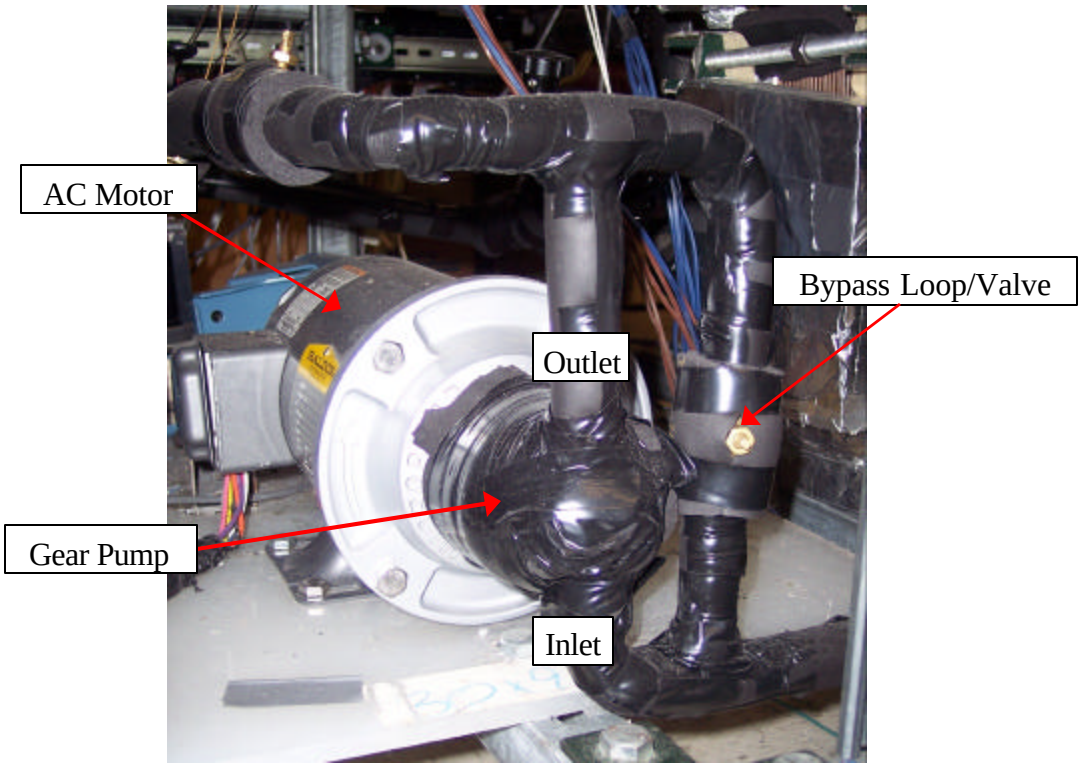

Figure 35 – AC Motor/Gear Pump Assembly and Bypass Loop

After the refrigerant flows through the pump, the 3/8" OD tubing splits into two paths: one with a filter-drier, the other without. The filter-drier is produced by Danfoss, P/N

DML-166s, and has 3/8" sweat connections. Each has a shutoff valve to block flow to that path. Both paths are constructed with 3/8" OD tubing throughout, and the paths are merged after the filter-drier. The flow then passes through the main mass flow meter, where the tubing is expanded with sweat connections to be 3/4" OD to match the 3/4" NPT connections at its inlet and outlet. The mass flow meter is a MicroMotion ELITE Coriolis-type mass flow meter, with 1/2" measuring tube diameter, and P/N CMF050M320NQBUEZZZ. The mass flow meters used in this study are described in detail in Section 3.2.1 – Mass Flow Rate Measurements. The outlet of the mass flow meter is then connected to the preheater. Figure 3 – Experimental Setup Schematic shows the system diagram between the pump and the preheater. Figure 36 is an image of the pump, main mass flow meter, filter-drier, and preheater as installed in the system.

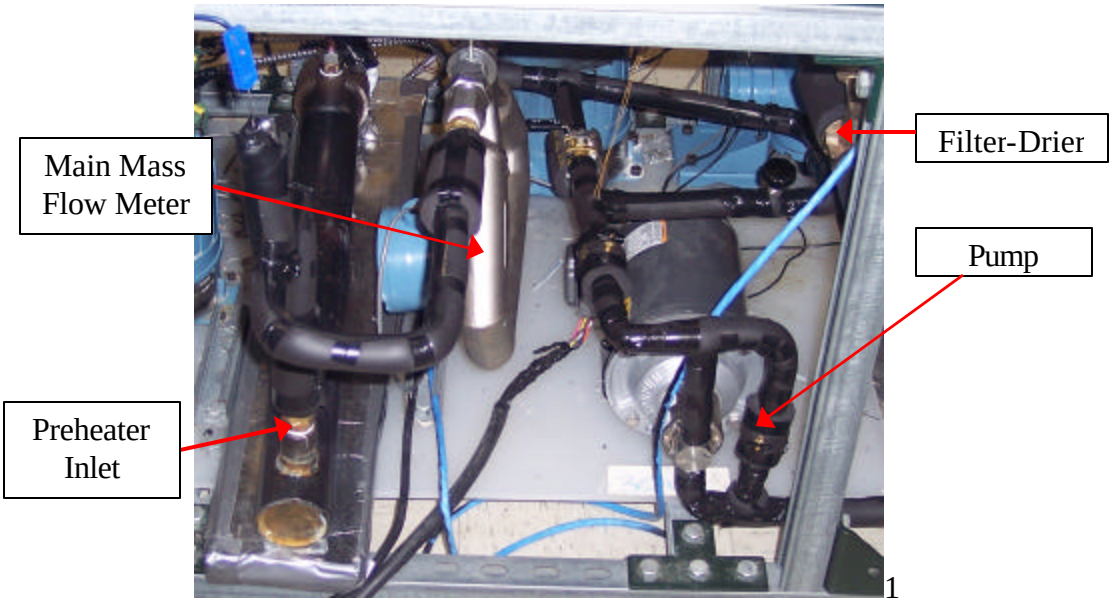

Figure 36 – Pump, Main Mass Flow Meter, Filter-Drier, and Preheater

3.1.2.9 Preheater and Visualization Section Inlet

The preheater consists of a cylindrical vessel with a 2-1/2" NPT threaded end, and an immersion heater cap. The heater cap is comprised of two 2.2 kW stainless steel immersion heating elements, the element's electrical connections, and a 2-1/2" NPT threaded male connection. The heating elements are contained in a 36" long cylindrical steel enclosure, with 3/4" NPT threads at each end, extending radially from the cylinder. The heating elements are used to evaporate the liquid flow from the pump into a two-phase flow with 30% vapor quality.

The exact heating capacity of the preheater is set with a voltage transformer, called a variac, which can change the voltage input to one of the 2.2 kW heater circuits. The other heating element is simply turned on or off, depending on whether the heating input needed is lower or higher than 2.2 kW. The variac used in this experiment is produced by Industrial Variac, P/N TDGC2-3KVA, and has a maximum power output of 3 kVA, or 3 kW. It is able to control a 110 volt, single phase AC power source, up to a maximum current of 30 amperes. Figure 37 is an image of a variac like the one used in this work.

Figure 37 – Voltage Transformer (Variac), 3 kVA, 110 VAC input

Once the two-phase flow exits the preheater, an absolute pressure measurement is made. This pressure is called either the visualization section inlet pressure or the evaporator inlet pressure. Simultaneously, two differential pressure measurements are made with two separate sensors. The first sensor measures the pressure drop across the microchannel heat exchanger, and the second measures the pressure drop across the inlet header/transparent tube of the visualization section.

The first sensor's tubing manifold is shown in Figure 26. The second sensor's manifold connects to the pressure taps on the bottom cover of the visualization section. The tubing for the manifold is entirely constructed of 1/4" OD copper tubing. Each of the ten pressure taps on the visualization section has a ball valve which is identical to the valves used in the manifold described in 3.1.2.3 – Microchannel Heat Exchangers. Figure 38 is an image of the manifold which measures pressure drop across the visualization header/transparent tube.

Figure 38 – Visualization Header/Transparent Tube Differential Pressure Manifold

After the differential pressure readings are made, the refrigerant flow out of the preheater is ready to enter the visualization section. Since the visualization section has two inlet locations, end and side, the 3/4" OD tubing is split into two separate flow paths. Each path has a shutoff valve similar to those used in the differential pressure manifolds, except that the connections are 3/4" NPT. The valves are sold by McMaster Carr, P/N 47865K24. Prior to entering their respective inlet to the visualization section, both flow paths have over 10 diameters of straight tubing to ensure fully-developed flow.

3.2 Measurement Devices and Data Acquisition System

This section describes the measurement devices used in the experimental and condensing unit systems, and the data acquisition system which is used to collect their outputs. This section also described the electrical systems used to control the heaters used in the experimental system.

3.2.1 Mass Flow Rate Measurements

The mass flow meters used in this work are all Coriolis-type mass flow meters, produced by MicroMotion. These Coriolis flow meters contain bent, vibrating tubes through which the measured fluid passes. The fluid accelerates as it flows toward the maximum vibration point, and slows down as it leaves that point. This causes the tubes to twist, and the amount of twisting is proportional to mass flow. Figure 39 shows the inner components of a MicroMotion sensor.

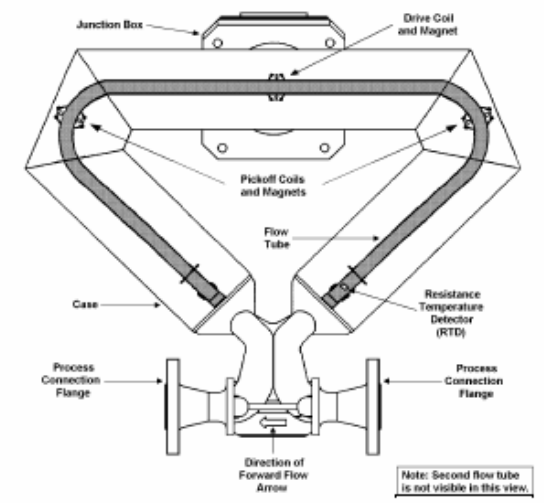

Figure 39 – MicroMotion Mass Flow Sensor Schematic Drawing, taken from MicroMotion CMF-series Product Manuals, www.micromotion.com

Each mass flow meter has two components: a sensor and a transmitter. The sensor contains the vibrating tubes, and sends a signal to its dedicated transmitter based on its

vibrations and temperature. A nine-wire data cable is used to transmit information between the components. The transmitter contains terminals for the data cable, power connections, and output wiring connections for the measured variables (mass flow rate, density, temperature). The transmitters can communicate with desktop computers using MicroMotion's proprietary software package, ProLink II, via a RS-485 protocol interface. The transmitters also produce a 0-5 volt DC output signal for mass flow rate which is read by the data acquisition system.

Three mass flow meters are used in the experimental system: liquid, gas, and main. The liquid and gas mass flow meters are both CMF025 models, meaning that the diameter of the vibrating pipe is 0.25 inches (1/4"). The nominal maximum mass flow rate of the sensor is 1090 kg/hr, or 303 g/s. The CMF025 sensors are each connected to their own MicroMotion 9739 series transmitter. The main mass flow meter is a CMF050, denoting a 1/2" diameter vibrating pipe, which has a nominal maximum mass flow rate of 3400 kg/hr, or 944 g/s. The CMF050 is connected to a MicroMotion 2700 series transmitter.

Using ProLink II, the transmitters can be programmed to improve the resolution of mass flow rate measurements by tightening the range of flow rates. For the liquid and gas mass flow meters, the transmitters are set to read between 0-60 g/s, and the main mass flow meter ranges from 0-75 g/s. Each of the three mass flow meters has calibration data that confirm accuracy to within 1% of the measured value. Calibrations were done using tap water, bucket & scale, and stopwatch. Figure 40 shows the graphs for these

calibrations. One final note on the mass flow meters used in this work is that they do not provide accurate or reliable data if the measured flow is two-phase.

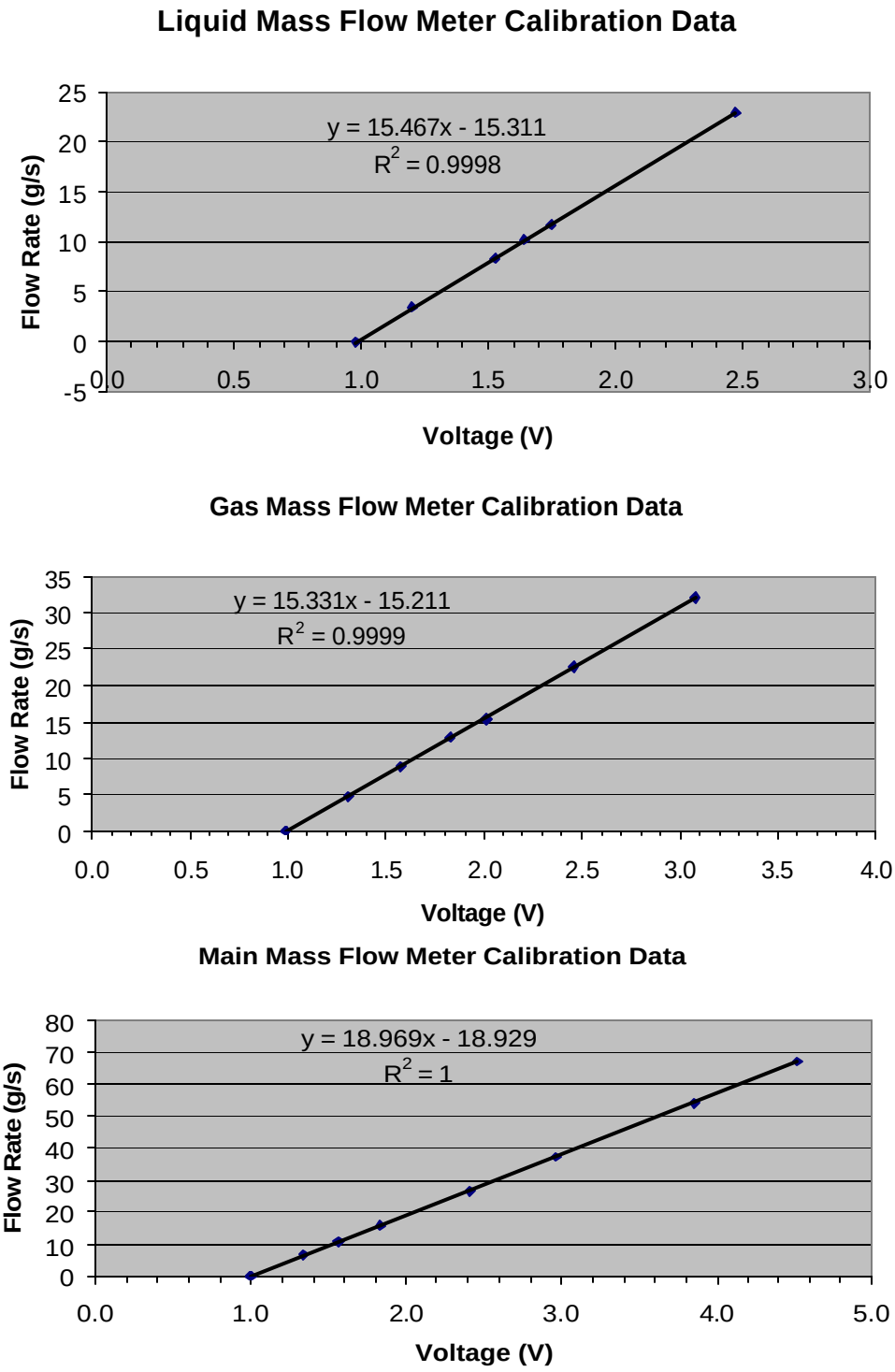

Figure 40 – Calibration Data for Experimental System Mass Flow Meters

3.2.2 Absolute Pressure Measurements

Absolute pressure measurements are made in both the experimental and condensing unit systems. Pressure measurements are made in the experimental system at the preheater outlet/visualization section inlet, and at the gas and liquid measured lines. In the condensing unit system, pressure measurements are made before and after the expansion valve. All of the pressure transducers used in this work are produced by Setra, P/N C207. Their specificed accuracy is ±0.13% full scale, including the effects of nonlinearity, hysteresis, and nonrepeatability. Each of the sensors is powered from the data acquisition system, which provides 24 volt DC power. The output of the transducers is 4-20 mA, corresponding to 0-250 psig. Figure 41 is a drawing of a transducer like the ones used in this work.

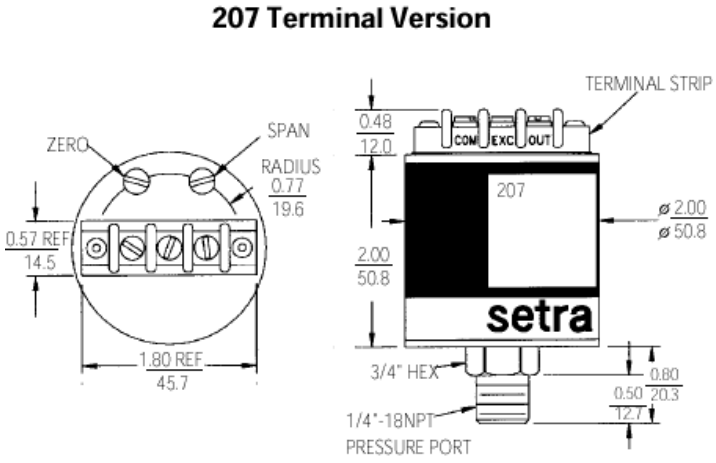

Figure 41 – Drawing of Setra C207 Pressure Transducer, with Dimensions in inches, taken from www.setra.com/tra/pro/pdf/206_207.pdf

Each of the pressure transducers used in this work have been calibrated with a digital pressure gauge over the entire measurement range of 0-250 psig. The calibration data

graphs mirror those of the mass flow meters in Figure 40, so only the calibration data are presented. These data are given in Table 3, next page.

Table 3 - Absolute Pressure Transducer Calibration Data

Transducer Location	Maximum Error (% Full Scale)	Average Error (% Full Scale)	R^2 value
Visualization Section Inlet	0.74	0.26	0.9998
Liquid Line	3.22	1.31	0.9985
Gas Line	0.51	0.29	0.9999
Expansion Valve In	0.64	0.39	0.9997
Expansion Valve Out	0.65	0.40	0.9997

3.2.3 Differential Pressure Measurements

A total of four differential pressure transducers are used in the experimental system, and none are present in the condensing unit system. Two of the differential pressure sensors are used to measure pressure drop across the visualization section. The first sensor measures the change in pressure between the visualization section inlet and the microchannel heat exchanger outlet, and has a range of 0-25 psid (psi differential). The second transducer measures the differential pressure between the visualization section inlet and the bottom cover pressure taps, and has a range of ±5 psid. The remaining two are used to measure the pressure difference between the measured and main paths for both the gas and liquid lines. Each of these sensors has a range of ±1 psid. This output is used to equalize the pressures in both lines by adjusting the needle valves in each line.

The sensors are all 230 series wet-wet transducers manufactured by Setra. The sensors are powered through the data acquisition system's 24 volt DC power supply. The output of the sensors is a 4-20 mA signal which is read into the data acquisition system. The

accuracy of the transducers is 0.25% of full scale, including nonlinearity, hysteresis, and nonrepeatability.

3.2.4 Temperature Measurements

Temperature measurements are conducted at many places in the experimental and condensing unit systems. There are three types of sensors, conventional thermocouples, in-stream shielded thermocouple probes, and ambient temperature sensors. All of the measurements are made using T-type thermocouples. Conventional thermocouples are accurate to within ±1ºC. However, it must also be considered that the temperature that is measured by a thermocouple is the surface temperature, not that of the refrigerant flow. The accuracy of the in-stream thermocouples is ±0.5ºC. The ambient temperature measurement is performed by the data acquisition system, and is accurate to within ±1ºC.

The condensing unit has temperature measurements at the following locations: compressor discharge, expansion valve inlet, expansion valve outlet, evaporator outlet, and compressor suction. These locations are shown in Figure 4 – Condensing Unit Cycle Diagram on page 14. Each of the temperature measurements is made with a thermocouple, placed on the outside of the copper tubing at that location, and insulated. These temperatures are recorded by the data acquisition system.

The experimental system has many temperature measurements, using both conventional thermocouple and in-stream probes. All energy balance calculations are performed using in-stream thermocouple measurements, due to their higher accuracy. Thermocouples are used to measure temperatures on the visualization section/microchannel heat exchanger

interface to protect the epoxy from high temperatures. A total of 30 thermocouples are placed on the microchannels, between the heating tapes and the top cover. These temperatures are not recorded by the data acquisition system, but are monitored by another system and incorporated into the heater control algorithm.

In addition, a total of 23 in-stream thermocouple probes are used in the experimental system. Figure 3 – Experimental Setup Schematic shows the locations of these probes. These temperatures are recorded by the data acquisition system. The probes used in this work are produced by Omega, P/N TMQSS-062U-6. Figure 42 is an image of a probe like the ones used in this work. The probes have 6" long stainless steel sheaths of 1/16" diameter, and have a quick-disconnect thermocouple connector at their end. The probes are installed in the system with 1/16" stainless steel compression fittings that clamp onto the thermocouple's sheath.

Figure 42 – Quick-disconnect Thermocouple Probe, with Stainless Steel Sheath, taken from www.omega.com/pptst/JMQSS.html

3.2.5 Power Measurements

The preheater consists of two heating elements and circuits, and each of these circuits is connected to a wattmeter. The wattmeters used in this work are produced by Ohio Semitronics, Inc., and their output is recorded by the data acquisition system. The first preheater circuit is connected to a GW5-020D wattmeter, with input ratings of 0-300 volts, 0-20 amperes, and output of 0-10 volts DC for the range 0-20 kW. This circuit is also controlled with the variac described in Section 3.1.2.9 – Preheater and Visualization Section Inlet. It is accurate to within ±0.2% reading, and ±0.04% full scale. The second circuit is connected to a PC5-059D wattmeter, with input ratings of 0-300 volts, 0-100 amperes, and output of 0-10 volts DC for the range 0-20 kW. It is accurate to within ±0.5% full scale.

3.2.6 Data Acquisition System

At the core of the study is a data acquisition system (DAQ) which reads in data from various analog signals and thermocouple wires. The system has two components, hardware and software, both of which are LabVIEW-based. The hardware used for data acquisition is a FieldPoint system based around a network module, and six input modules each with eight input channels. All of the hardware is manufactured by National Instruments. The network module is a FP-1000, with a RS-232 serial connection that transmits all data to the DAQ computer. Of the six input modules, two are AI-110 modules, which are used for reading analog voltage (0-10 DC) or current (0-20 mA) input signals. The remaining four input modules are TC-120 models, which are used to record thermocouple temperatures, in addition to an ambient temperature measurement.

Each of the modules has a TB-3 terminal base with 32 screw connections for input wiring. The modules are powered with a 24 volt DC power supply, and this power source is cascaded to the two AI-110 modules. Each of the modules then provides power to individual sensors and measures their output. The thermocouple modules do not require power. Figure 43 is a photograph of the modules as installed in the system.

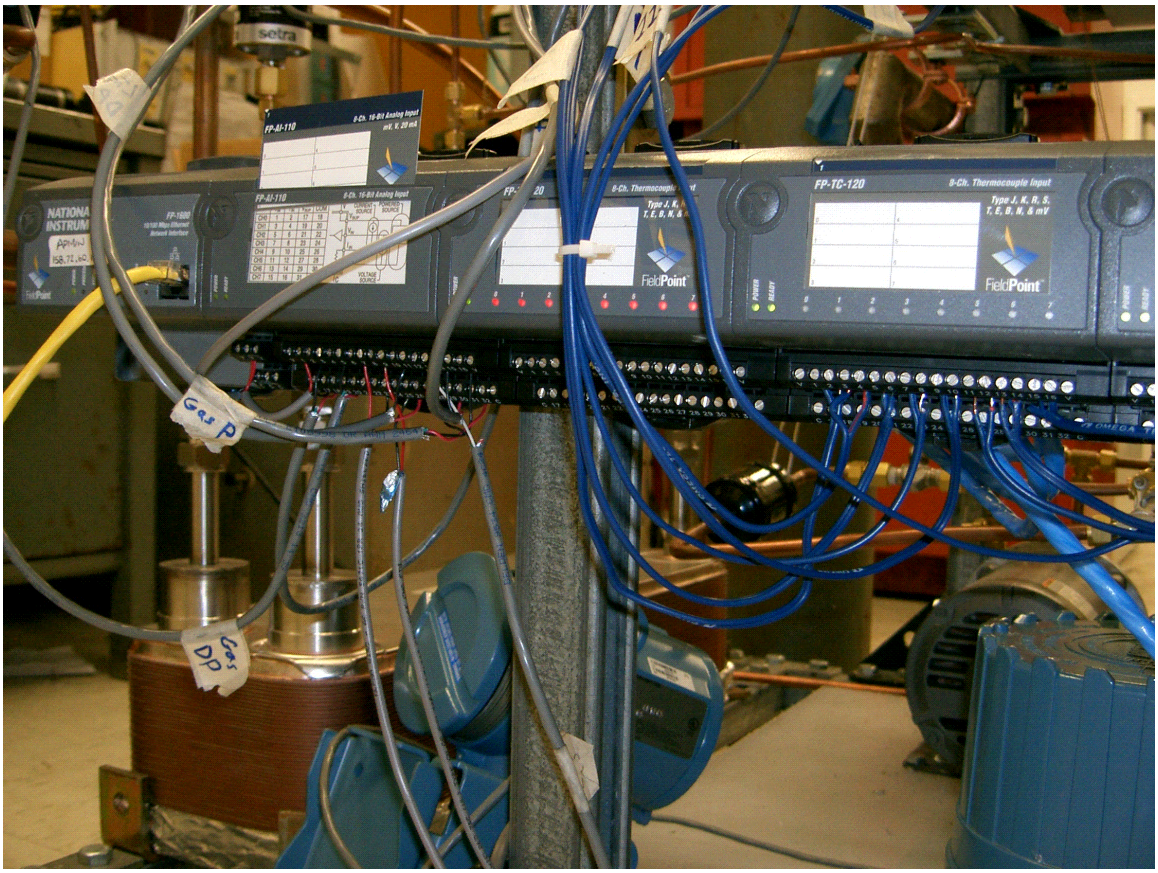

Figure 43 – Data Acquisition System – FieldPoint module setup

The software component of the DAQ is a LabVIEW program which takes the raw data values from the FieldPoint modules, and converts them to useful data. For example, a 6 mA signal from a pressure transducer is converted to a 62.5 psi pressure reading using user-defined equations. These equations are either taken from calibration data, or if no calibrations are available, from the manufacturer's data. The software's user interface

consists of tools to change the sampling time, the output path for saved data, enabling or disabling writing data to disk, and stopping or starting sampling. Also, the DAQ interface allows the user to indicate which flow branch's mass flow rates and pressure drops are being monitored, by using a slider which goes from zero to ten in integer increments. Zero is used for general measurements, where no flow branch is being isolated. The user interface also continuously displays the data which is being received from the FieldPoint modules, both in graph and number format. Figure 44 is a screen shot of the DAQ user interface.

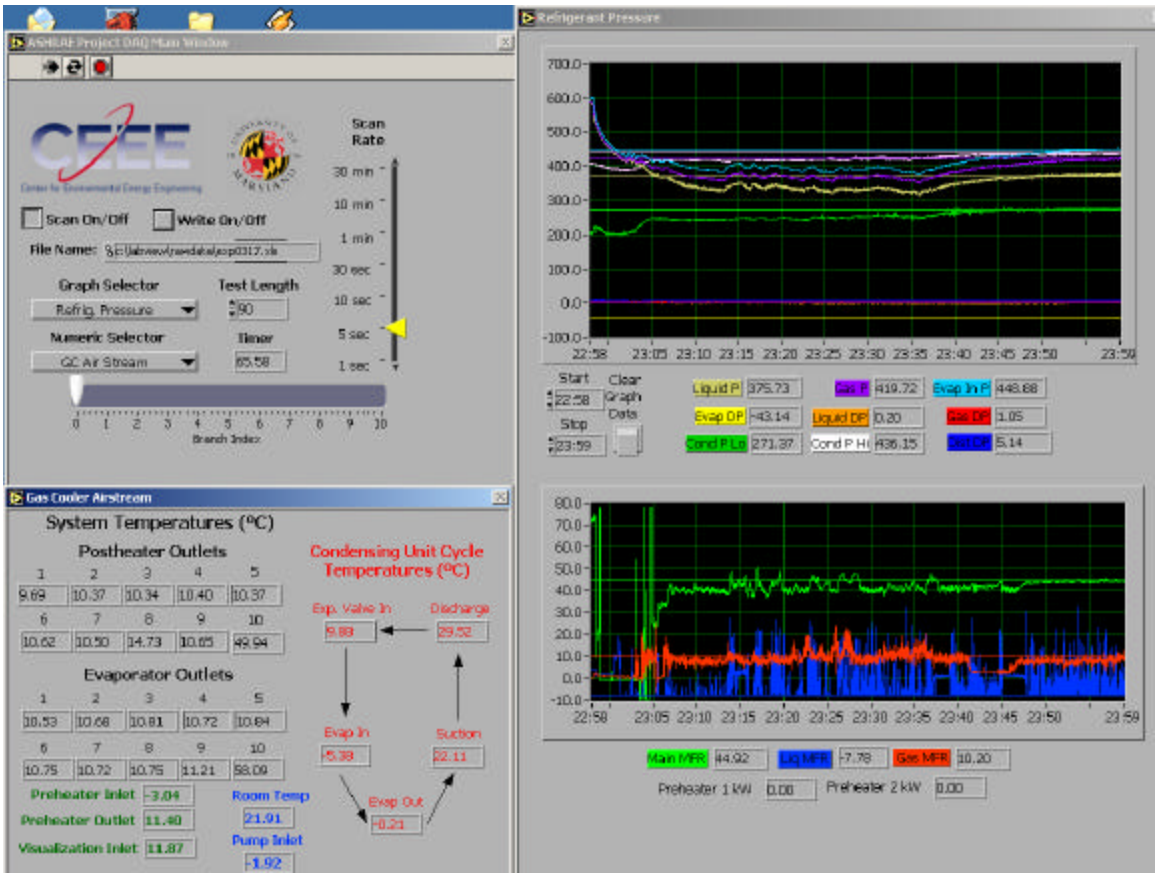

Figure 44 – Data Acquisition System – LabVIEW User Interface

All data which is recorded by the DAQ is exported to a Microsoft Excel template, and plots of important variables are automatically generated – mass flow rates, flow

distribution, absolute pressures, and temperatures. These data files are then catalogued by date, and stored on disk.

3.2.7 Energy Balances

There are two main energy balances which are used in this work, both of which are within the experimental system cycle.

The first energy balance is applied over the preheater to ensure that the visualization inlet receives an inlet flow with 30% vapor quality. At the inlet, the temperature and mass flow rate is known, and the fluid is a subcooled liquid. At the outlet, the temperature and pressure are known. The power input to the preheater is also known. The power input is adjusted to obtain the desired outlet vapor quality. It is assumed that the enthalpy of the inlet flow is unchanged due to pressure differences between the preheater inlet and outlet. The impact of a 30 kPa pressure difference on the energy balance is less than 1%. Table 2 shows the equations used to determine the power input to the heater.

Table 4 - Energy Balance Equations for Preheater

$$p_2 = \mathbf{P}('R134a', T=T_2, x=x_2) \quad (1)$$

$$h_2 = \mathbf{h}('R134a', T=T_2, x=x_2) \quad (2)$$

$$p_2 = p_1 \quad (3)$$

$$h_1 = \mathbf{h}('R134a', T=T_1, P=p_1) \quad (4)$$

$$Q_{12} = \dot{m} \cdot (h_2 - h_1) \quad (5)$$

The second energy balance is computed for each of the 10 heat exchanger branches, and used to calculate the quality of each flow under heat input conditions. The balance begins at the entrance to the visualization section. As stated above, pressure,

temperature, mass flow rate, and vapor quality are all known at this point. Then, the flow is distributed in the transparent header, and the flows pass through the microchannel heat exchanger. The input energy which is applied to each group of microchannels is known via on-off time ratio and tabulated resistances for each group of tape heaters. At the outlet of the heat exchanger, the temperature of the flow is measured by an in-stream thermocouple. If the flow is superheated vapor, then the energy balance is computed with the mass flow rate measured by the gas mass flow meter, and the gas pressure. If the flow is two-phase, the energy balance is computed with the outlet vapor quality, which is found by measuring the liquid and gas mass flow rates. In addition, the liquid and gas pressures are considered when determining outlet enthalpy. This is done for each of the 10 outlets of the heat exchanger, until the quality distribution and mass distribution of the entire control volume is found. Finally, the energy at the inlet plus heating input is compared to the outlet conditions.

3.2.8 Heater Controls

The preheater and microchannel heating tapes are potentially dangerous objects, and must be controlled to prevent overheating episodes. Therefore, each is equipped with a safety control box which prevents power from being supplied if the heaters exceed safe temperature setpoints. The preheater is controlled with an on-off controller which is produced by Omega, P/N CN76000. The controller is given a temperature setpoint by the user, and connected to the preheater outlet in-stream thermocouple probe. The controller output is connected to two 25 amp solid state relays which are also produced by Omega, P/N SSR330DC25. When the temperature is below the setpoint, a 9 volt DC signal is sent to the relays, and the relay terminals connect. This allows the preheater circuit to

receive power. If the temperature exceeds the setpoint, the relays do not receive power, and the heater circuits cannot receive power. Each of the relays is mounted on a heat sink which is rated at 1.5 W/ºC, to ensure that overheating of the relays does not occur. The heating tapes on the evaporator are also controlled by 12 solid state relays, which are contained in one electrical box. Each of the relays has its own heat sink, and its own DC control voltage line which connects to a Hewlett-Packard data acquisition system. It is important to note that this data acquisition system (DAQ) is not the main DAQ for this work, but rather it is used only to control the heating tapes on the evaporator. This system reads in the temperatures from the microchannel heat exchanger outlet thermocouples, and also from the thermocouples which protect the epoxy on the top cover. If any of the temperatures exceed the setpoints for safety, the heating tapes for that particular group are shut off. This is done with an actuator card, which either opens or closes the DC power circuit to that particular heating tape group's solid state relay. Each of the 12 relays can be turned on or off independently, and once the temperatures return to a safe level, the relay operates as usual. If the system temperatures are at safe levels, then the relays/heating tapes are turned on and off depending on the fractional-on-time that is specified by the user. One complete program cycle takes approximately two seconds, so a 50% on-time ratio results in repeated cycles of two seconds on, two seconds off.

It should be noted that there are more relays than groups of three microchannel heating tapes, and this is because of electrical constraints related to the building circuitry. A total of six electrical circuits are used to provide power to the heating tapes, five of which are

20 ampere circuits, and one which is a 30 ampere circuit. A group of three heating tapes draws 12 amperes of current, meaning that only seven circuits of three heating tapes are possible with the electrical capacities on hand. The remaining nine heating tapes are spread out over five relays, and controlled in groups of one or two. All of the relays are connected to their respective heating tapes with power cables and wire nuts. The wiring diagram is shown below, in Figure 45. The bottom numbers correspond to the 30 heating tapes used in the system. The middle numbers refer to the relays which control each group of tapes. The top numbers denote power connections made to the room's electrical supply.

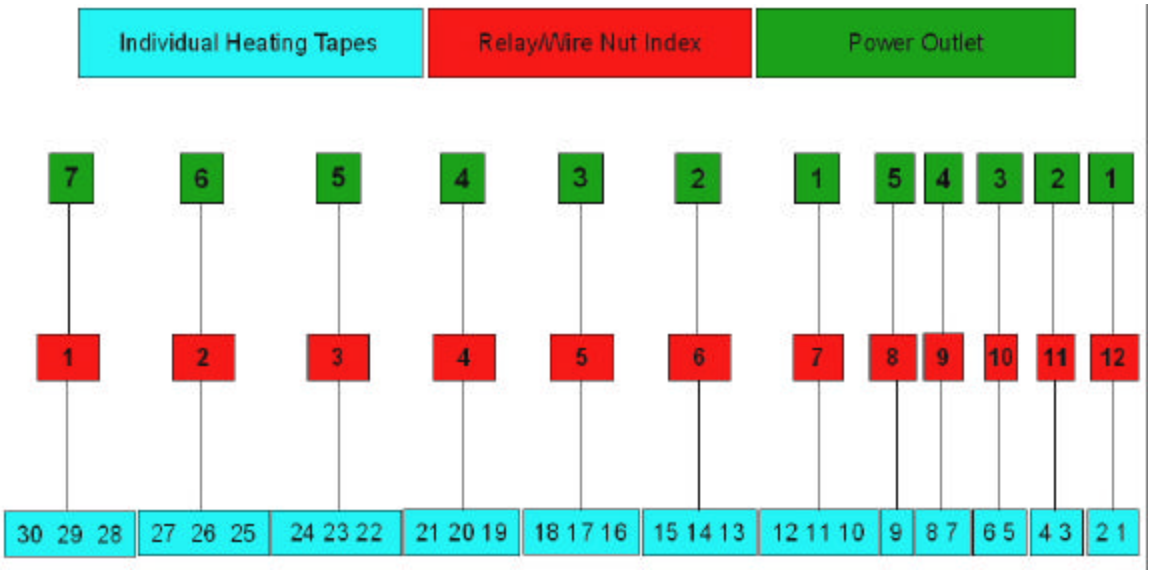

Figure 45 – Wiring Diagram for Heating Tapes and Solid State Relays

4 Experimental Procedure

This section contains descriptions of the procedures used to meet different test conditions. These procedures fall into two basic categories: setup and runtime. Setup procedures are performed while the system is not running. Runtime procedures are used during system operation.

4.1 Setup Procedures

4.1.1 Tube Pitch

Three microchannel heat exchangers are used in this work, with tube pitches of 8, 10, and 12 mm. In order to switch between the different pitches, the following components must be changed: top cover/heat exchanger, bottom cover, transparent tube, and support blocks. Each of these components has three designs, corresponding to the three tube pitches. Heating tapes must also be installed on the microchannels for the installed pitch.

4.1.2 Tube Number

The number of parallel tubes in use at a time can be set as either 18, 24, or 30. A set of dead blocks are inserted into the transparent tube to block the flow to a particular group of microchannels. The dead blocks are sized to block 6 and 12 tubes for end inlet conditions, and 3 and 6 tubes for side inlet conditions. In side inlet cases, the dead blocks are used on both ends of the transparent header. Also, when tube number is reduced, the heating tapes which are located on the dead paths of the heat exchanger must have their power disconnected.

4.1.3 Refrigerant

Two working fluids are used in this work, R134a and R410A. Switching between refrigerants is done using a recovery unit and designated recovery cylinders for each fluid. Once all of the refrigerant has been recovered from the system, a vacuum pump is used to fully evacuate the system. The system is then ready to be charged with a new refrigerant.

4.1.4 Heat input

The heat input across the microchannel heat exchanger is controlled automatically during testing, as described in Section 3.2.8. However, the fractional on-time and cycle time must be set in the data acquisition system which controls the heaters. The factors which determine these settings are tube number (18, 24, 30 ea) and heat load (0, 5, 10 kW). Table 5 contains sample calculations for fractional on-time. N_{tube} is the tube number, Q_{max} is the total heating capacity of the heating tape array, and Q_{req} is the heat load condition.

Table 5 – Heating Tape Fractional On-time Calculations

N_{tube} [ea]	Q_{max} [kW]	Q_{req} [kW]	Fractional On-time
18	8.4	5	0.59
18	8.4	10	1.00
24	11.2	5	0.45
24	11.2	10	0.89
30	14.0	5	0.36
30	14.0	10	0.71

4.2 Runtime Procedures

4.2.1 Inlet Location Control

The visualization section has two inlets: side and end. Switching between the two is done by simply closing the valve at the previous inlet location, and opening the valve at the new inlet location.

4.2.2 Mass Flow Rate Control

The main mass flow rate of the experimental system can be set to 30, 45, or 60 g/s. Two methods are used to control mass flow rate during system operation, a bypass loop, and an in-line metering valve. Both are sized so that at peak, the mass flow rate in the system exceeds 75 g/s. When the controls are used, the mass flow rate can be lowered to 30 g/s. The pump and bypass loop assembly is shown in Figure 35.

4.2.3 Absolute Pressure/Temperature Control

Controlling the absolute pressure and temperature at the preheater inlet is done by adjusting the capacity and temperature of the condensing unit cycle evaporator. If a lower pressure is needed in the experimental system, the capacity of the condensing unit system is increased by closing the hot gas bypass. If a lower temperature is needed, the expansion valve in the condensing unit cycle is closed more. Both of these methods work in reverse, if the temperature or pressure in the system needs to be increased. In general, only the pressure is controlled, since the preheater allows for flexibility in heating the refrigerant flow into the visualization section. Figure 8 shows the components which are used to control the capacity of the condensing unit.

4.2.4 Vapor Quality Control

The preheater inlet and outlet conditions are constantly monitored, and an Engineering Equation Solver (EES) program provides the correct heating input required to heat the outlet flow to a 30% vapor quality, based on the energy balance described in Section 3.2.7. Based on this number, the variac which controls the preheater capacity is adjusted, and a wattmeter records the power input. The process is conducted until steady-state conditions are obtained at 30% vapor quality.

4.2.5 Branch Measurement

During testing, the mass flow rates and pressure drops for each flow path are measured independently. A total of four measurements are made for each branch: liquid mass flow rate, gas mass flow rate, heat exchanger pressure drop, and header pressure drop. The manifolds for pressure drop are set up such that one out of ten valves is open. The valve which is open is the measured branch. Switching between branches is done by simply opening a new valve and closing the valve which was previously measured. Figure 26 is an image of one of the differential pressure manifolds that is adjusted in this way.

Similarly, for mass flow rate measurements, both the liquid and gas outlets of the phase separators are connected to three-way valves. These three-way valves either route the flow into the main flow, which is fed by nine of the ten branches, or into the mass flow meter. Switching between branches is done by rerouting the measured flow into the main flow, and switching the valve setting on the new measured branch. Figure 30 is an image of the flow branches and three-way valves as installed in the system.

In the data acquisition system user interface, a slider is used to set "Branch Index" to any integer from 0 to 10. This slider is shown in Figure 44 near the bottom of the top left window. If the system is not ready for measurements of mass flow rate and pressure drop, then 0 is used. Otherwise, the slider is set to the same number as the index of the branch which is being measured. The slider is changed after a satisfactory number of data points are recorded for a given branch, and only then are the valves in the system changed. Later, the data are reduced in Microsoft Excel such that only the last 20 data points from each branch are used in mass flow rate distribution and other analyses.

5 Flow Visualization

One of the primary goals of this work is the direct visualization of the flow through a realistic multiport header of a microchannel heat exchanger. The design and construction of the visualization section used in this work is described in Section 3.1.2.2. Personal inspection and video acquisition can be achieved through the sight glass of the visualization section. This chapter describes the video acquisition hardware and software that are used to visualize the flow, and gives still images from trial runs of the system.

5.1 Video Acquisition

For each test, video is recorded through the use of a digital camcorder. The camcorder used in this work is a Sony MiniDV camcorder, P/N DCR-TRV33. Figure 46 is an image of the digital camcorder.

Figure 46 – Digital Camcorder for Video Acquisition

The camcorder has 690,000 video pixels, 10x optical zoom, 120x digital zoom, and has FireWire capability for streaming video. A 30 mm circular polarizing filter is used to reduce reflections in the video, and allow for clearer inspection of the flow. This lens is produced for Sony camcorders, P/N VF-30CPKS. The video stream is output to the data

acquisition computer, which uses Windows Movie Maker for video review and editing. A DVD-R drive is used to record video to DVD media for storage. Figure 47 and Figure 48 are two images taken from a video of a side inlet test with the following conditions: R134a, 30 g/s, 10 mm tube pitch, 30 tubes in parallel. Each figure contains two copies of the same image, one with an indicated liquid level, and one without. Both images are taken from the same test video, a few seconds apart.

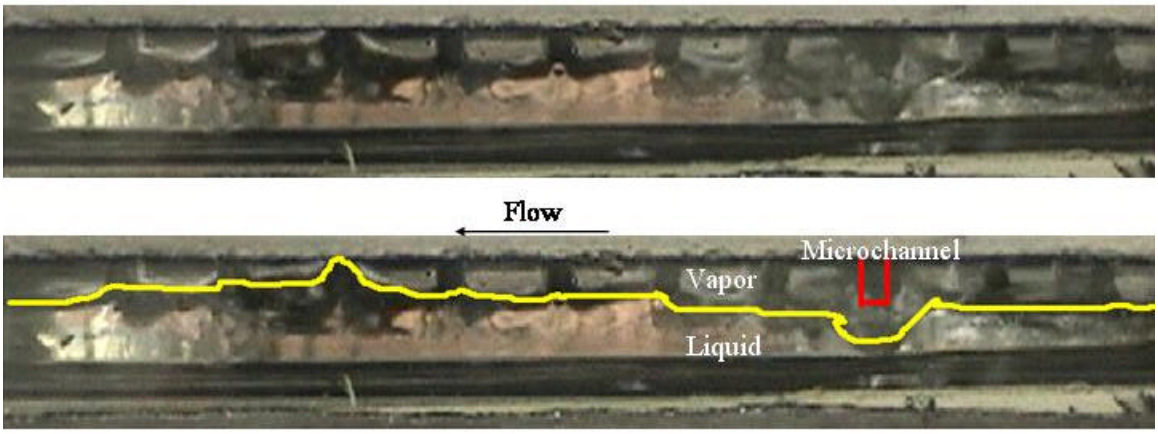

Figure 47 – Sample Image of Flow Visualization, Side Inlet, 30 g/s, R134a, 10 mm Pitch, 30 Tubes

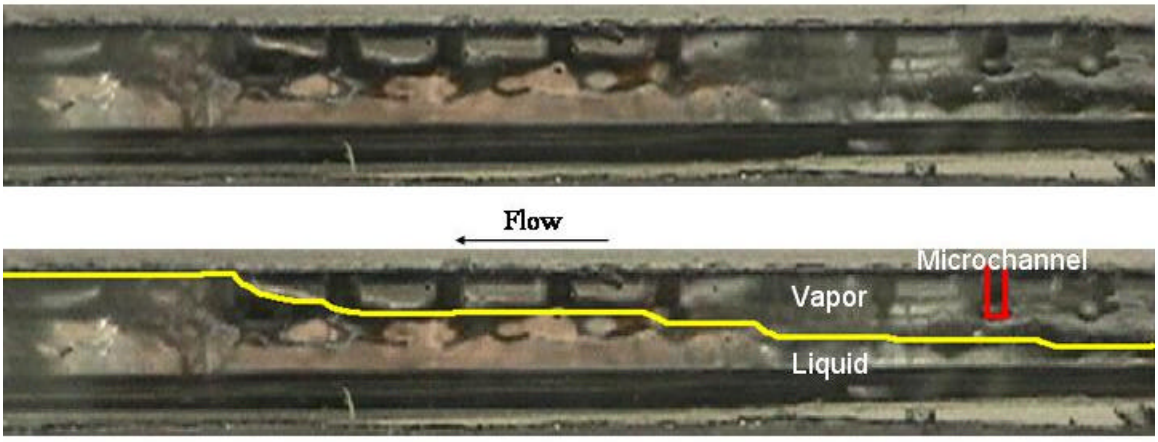

Figure 48 – Sample Image of Flow Visualization, Side Inlet, 30 g/s, R134a, 10 mm Pitch, 30 Tubes

Still images from the digital camcorder are not very descriptive, as it is only a 1 megapixel camera. However, flow videos very clearly show that maldistribution is

present in the header. The liquid level at the last group of microchannels on the left is above the microchannel ports, whereas the liquid level is very low near the inlet (on the right). Between the two extremes, the flow is turbulent and the liquid level surges and recedes with a frequency in the range of a few seconds.

6 Results and Discussion

This section presents and discusses the results of preliminary tests conducted to verify the experimental setup's utility. The experimental setup is able to meet the test conditions at the visualization section inlet, including pressure, temperature, and vapor quality. Although no full set of distribution data exists to back-check the vapor quality, flow visualization and energy balances result in only a ± 0.4% uncertainty for the desired 30% inlet quality to the evaporator. An uncertainty analysis of this energy balance can be found in Section 9 - Uncertainty Analysis. The system operates at stable pressure, temperature, and main mass flow rate conditions under adiabatic conditions for extended periods of time.

Unfortunately, no full set of maldistribution data exists, due to phase separation problems, and resultant two-phase flow through the liquid and gas mass flow meters. As discussed in Section 3.2.1, Coriolis mass flow meters cannot measure a two-phase flow with any real accuracy. However, limited data from low heat load tests indicate that the phase separators are functional at high vapor qualities and superheated vapor inlet conditions. The mass flow rates from such flows are steady and reasonable, and indicate that full data sets are obtainable under 5 and 10 kW heat load conditions.

Three diagnostic test runs illustrate the impact of heat load. The first test run has no heat load except for the final group of 3 microchannels, Group 1, which are heated at 20% of full power. On average, the three microchannels receive a total of 280 W, corresponding to a 2.8 kW heat load condition if extrapolated over the entire heat exchanger. Figure 49

is a plot of mass flow rate over time. The gas and liquid mass flow rates shown in the figure are measured only for the heated group of microchannels. After the microchannels begin receiving heat input, the gas mass flow reading for Group 1 is 2.1 ± 0.25 g/s. The liquid mass flow rate is not meaningful, as the reading of -7.78 g/s corresponds to the error signal, 2 milliamperes. This error signal is typically observed when a two-phase flow is being pushed through the mass flow meter. Therefore, it is not possible to know the inlet or outlet vapor quality of Group 1 due to the unreliable liquid mass flow reading. An important result of this test is that the phase separators can output a pure gas from the vapor outlet while simultaneously producing a two-phase flow at the liquid outlet.

No superheating was observed, as shown in Figure 50, which shows the microchannel heat exchanger outlet temperatures during this test. During the test, the outlet temperatures increase by 2ºC, but all 10 groups' outlet temperatures are collinear. Since the inlet quality is less than 30%, it is reasonable to assume that all 10 groups have two-phase flow at their outlet.

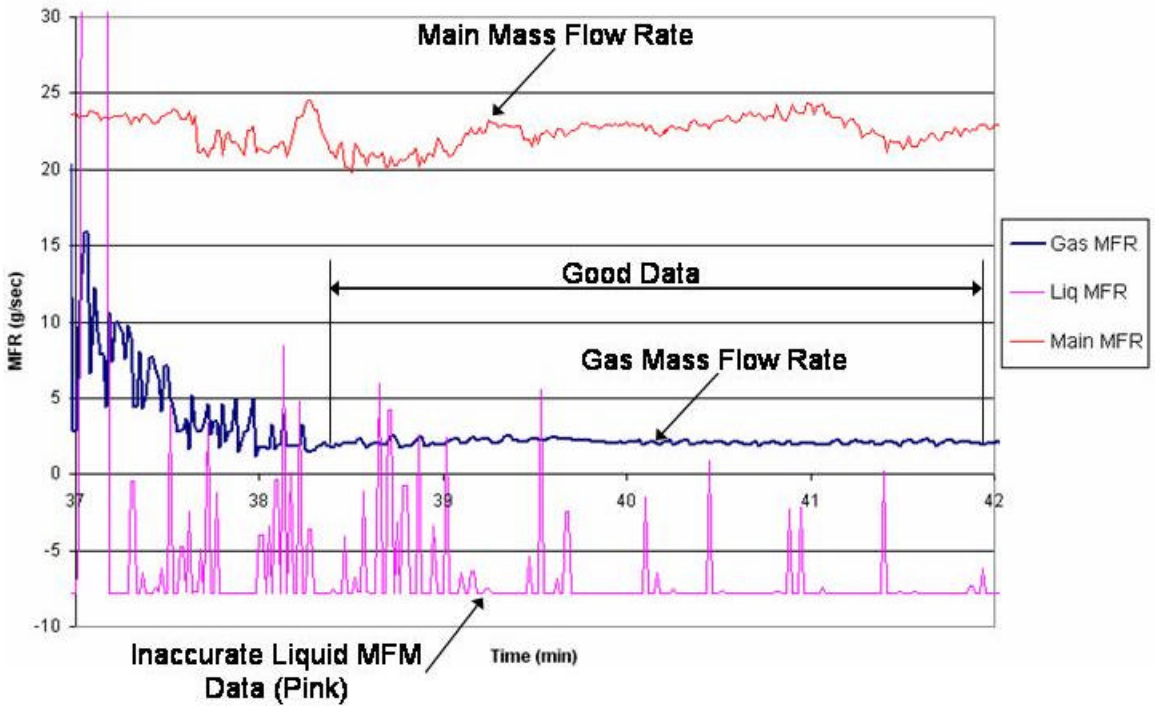

Figure 49 – Mass Flow Rates, Group 1 heated, 20% Power, R134a

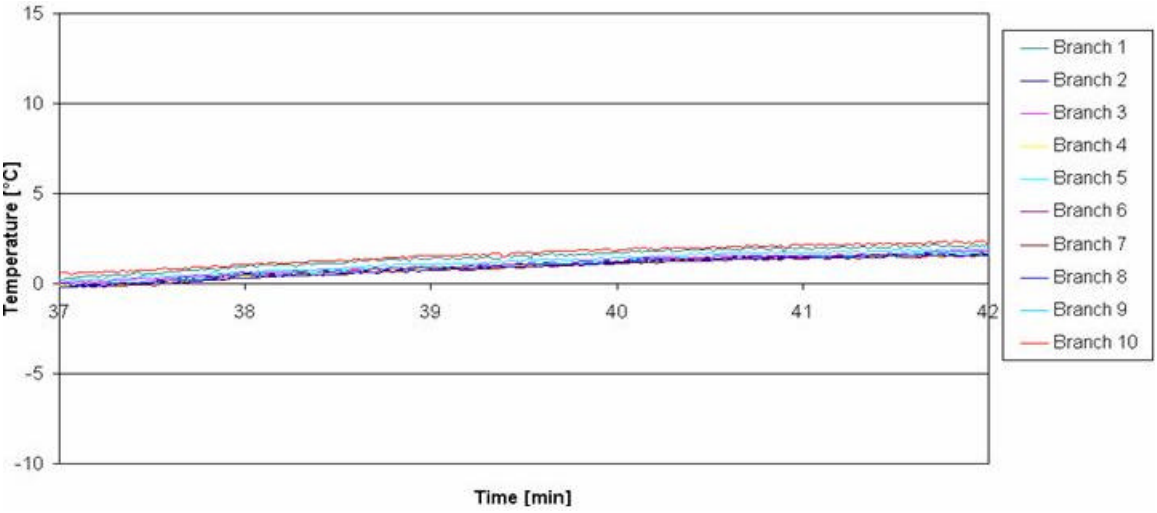

Figure 50 – Temperature Profile of Microchannel Heat Exchanger Outlets, Group 1 heated, 20% Power, R134a

Due to its location at the far end of the header, the inlet flow to Group 1 is almost entirely liquid. This liquid condition is confirmed both by visual inspection, as shown in Section 5 – Flow Visualization, and in previous studies by Vist (2004) and others. However, due to a lack of insulation on the bottom cover and attached tubing during this test, evaporation was occurring in the differential pressure manifold below the transparent

tube. As a result, bubbles floated upward from the bottom cover, through the transparent tube, and into the microchannels. The inlet quality can therefore be assumed to be higher than during a normal, insulated test, in the range of 20-30%. It should be noted that the inlet to the visualization section is not at 377.5 kPa and 7.2ºC, the target test conditions. The inlet temperature is 2.5ºC at minute 40, as shown in Figure 51. The inlet pressure is 334 kPa at the same time, which corresponds to a saturation temperature of 3.3ºC. This temperature is within a degree of the measured temperature, so it can be assumed that the fluid is at 3.3ºC. The system pressures can be seen in Figure 52. Flow visualization confirms this assumption. At the same time, the outlet temperature is 1.7ºC. In the absence of superheating, we can calculate the outlet pressure as the saturation pressure at 1.7ºC, which is 312 kPa. This agrees well with the measured pressure at the gas mass flow meter, which is 313 kPa. The vapor mass flow rate is measured as 2.1 g/s.

Using the measured values of temperature, pressure, vapor mass flow rate, heating input, and assuming a 30% liquid flow at the inlet to Group 1, an energy balance can be performed. The inlet enthalpy is calculated to be 115.5 kJ/kg, and the outlet enthalpy is 249.2 kJ/kg. The energy balance indicates that 1.5 g/s of liquid is evaporated in Group 1. This number is then combined with 0.6 g/s of vapor which entered as bubbles from the bottom cover to reach the gas mass flow meter reading of 2.1 g/s. This demonstrates that the values measured by the gas mass flow meter are reasonable, as is the energy balance. As mentioned above, it is not possible to know the exact quality at inlet or outlet due to the lack of a liquid mass flow reading.

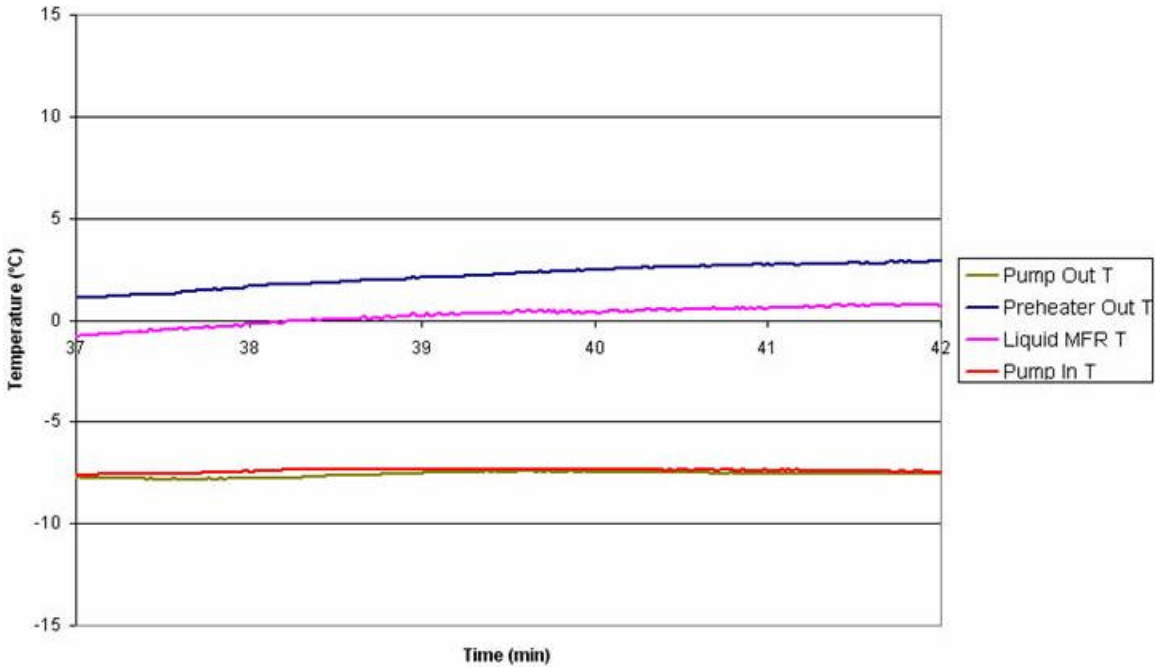

Figure 51 – Pump, Preheater, and Liquid MFM Temperatures for Group 1 Heated, 20% Power, R134a

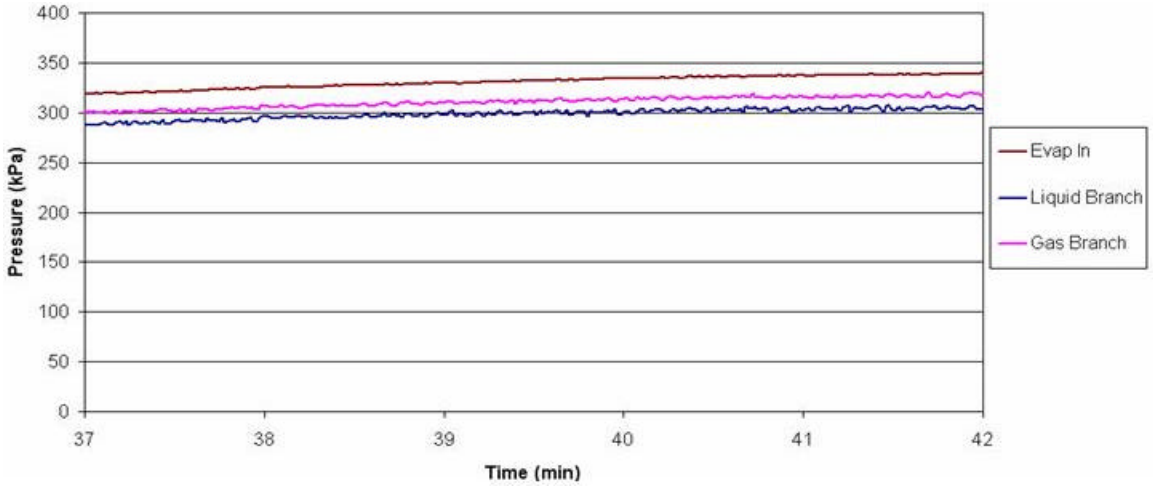

Figure 52 – System Pressures for Group 1 Heated, 20% Power, R134a

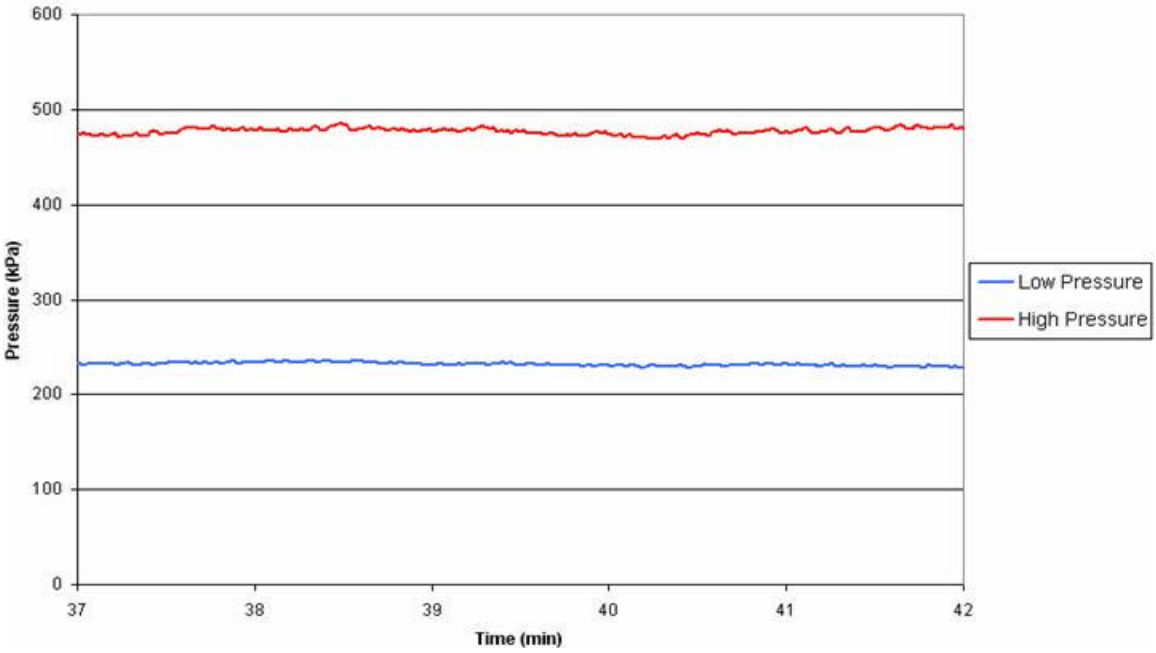

Figure 53 – Condensing Unit Pressures for Group 1 Heated, 20% Power, R134a

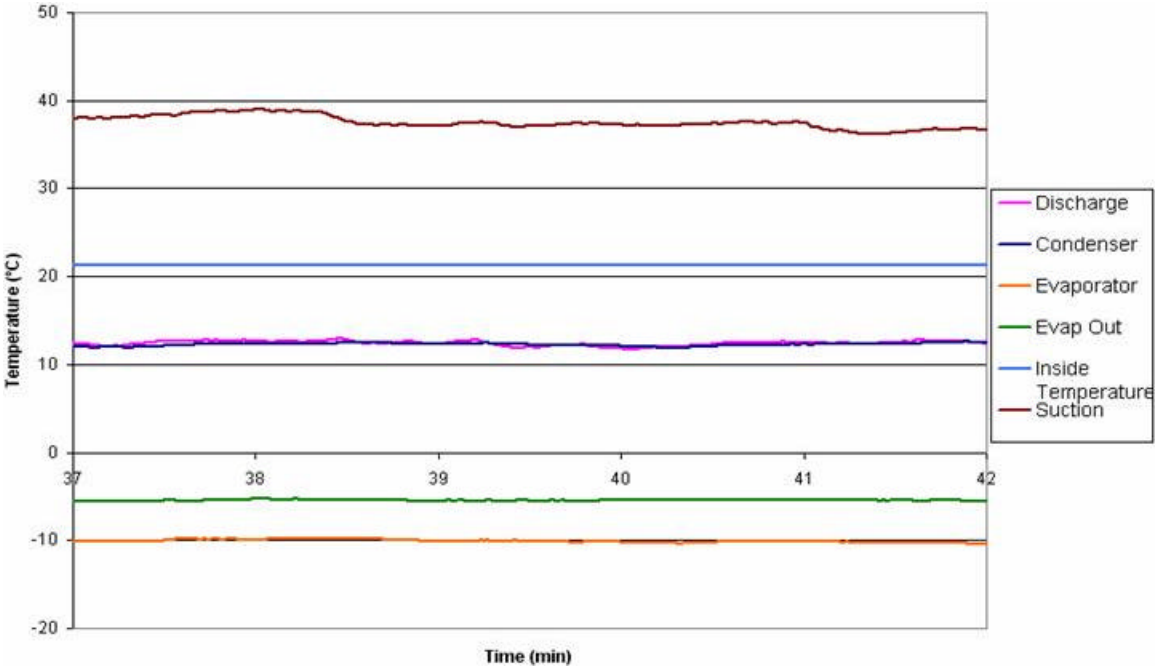

Figure 54 – Condensing Unit and Room Temperatures for Group 1 Heated, 20% Power, R134a

Figure 53 and Figure 54 show the operating pressures and temperatures for the condensing unit cycle. Although there are changes in the condenser temperature and high pressure, the evaporator inlet and outlet temperatures remain very stable. These

condensing unit cycle data support the temperature data in Figure 51, showing the stability of pump and preheater inlet conditions in the experimental system.

The first test proves the impact of heating tapes on improving phase separation after the microchannel heat exchanger. However, the liquid mass flow rate is unsteady, suggesting that the flow through the liquid mass flow meter is two-phase, due to poor phase separation. The second test shows that phase separation can be improved by further raising the inlet vapor quality to the phase separators. This test is identical to the first, except that the heating tape was set to 20% power, as before, and then increased to 100% power for about a minute. At 100% power, the heat input to the three microchannels is 1.4 kW. Figure 55 is a plot of the mass flow rates, and Figure 56 is a plot of the temperature profile at the heat exchanger outlet.

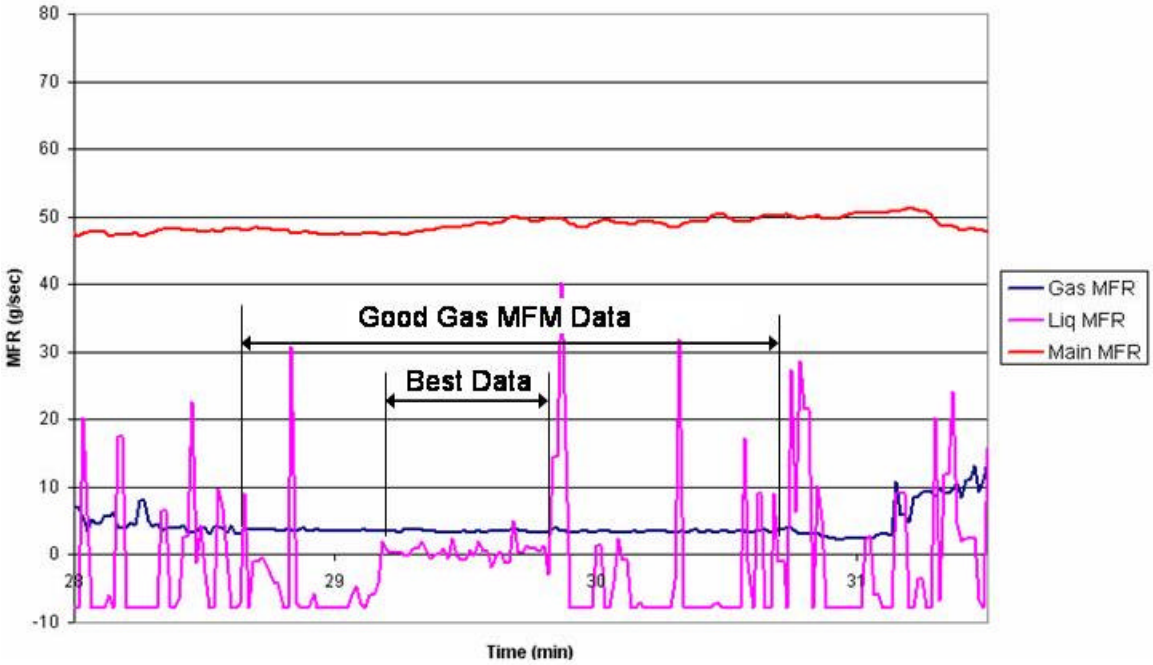

Figure 55 – Mass Flow Rates, Group 1 Heated, 20-100% Power, R134a

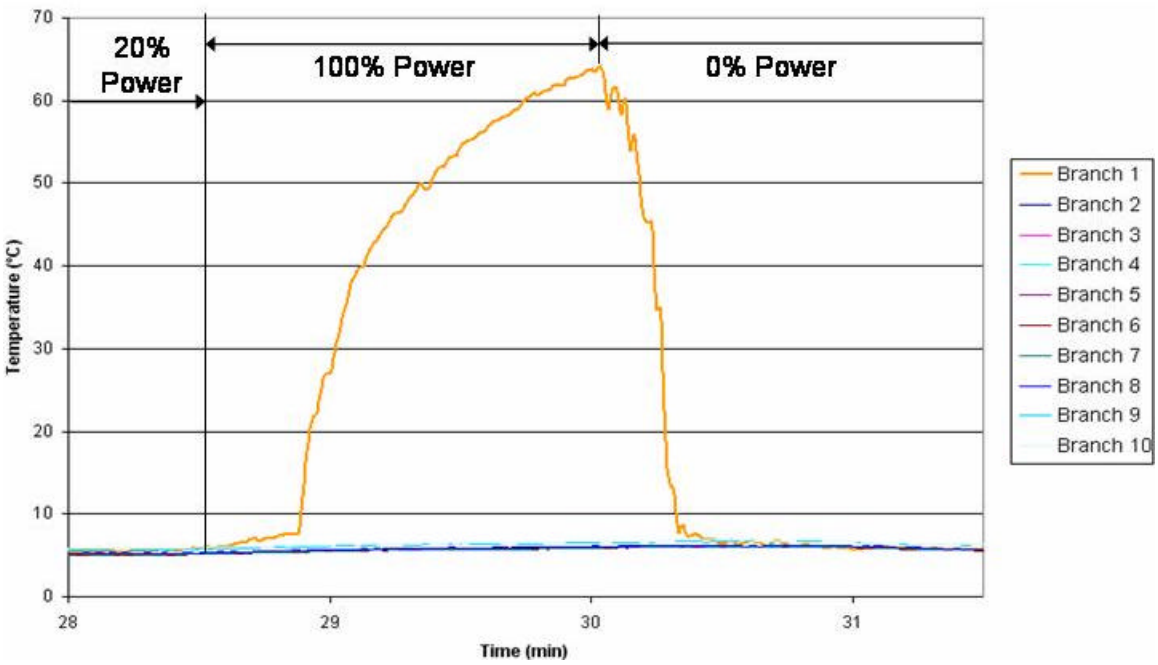

Figure 56 – Temperature Profiles of Microchannel Heat Exchanger Outlets, Group 1 heated, 20-100% Power, R134a

With 20% power for the heated microchannels, the gas mass flow rate is steady and reasonable, similar to that which was observed in the first test. The liquid mass flow meter still received two-phase flow, however, and did not provide a good reading. When switched to 100% power, the microchannel flows became superheated, and no phase separation was necessary. Under these conditions, the average liquid mass flow rate is zero, although it is oscillatory, and ranges between ±2 g/s. The system, although not at steady-state, can be analyzed at 29.5 minutes for operating conditions and energy balance purposes. At this time, the preheater outlet temperature is shown in Figure 57 to be 7.0ºC. The pressure is measured as 390 kPa, as shown in Figure 58. The saturation temperature for this pressure is 8.1ºC, which is assumed to be the true inlet temperature for enthalpy purposes. The outlet temperature is measured as 54.4ºC, and the absolute pressure at the gas mass flow meter is 361 kPa. The gas mass flow meter gave a reading of 3.6 g/s, and the liquid mass flow meter reads -0.77 g/s. However, since the liquid mass

flow meter gives a reading of +0.74 g/s the next second, these numbers are averaged to give a zero mass flow rate. In addition, if all 60 of the liquid mass flow rate readings for the range 29-30 minutes are combined, the average liquid mass flow rate is -0.02 g/s. The total mass flow rate through the evaporator is measured as 48.7 g/s.

An energy balance calculation shows that much of the power of the heating tapes is lost to the environment. If the heat was entirely absorbed by a 3.6 g/s liquid refrigerant flow, the outlet temperature would be over 400ºC. The percent of the total heating energy which is received by the refrigerant is 60% at 29.5 minutes. The remaining energy is lost to ambient air, since the microchannels were not insulated. The surface temperature of the microchannels exceeded 100ºC when measured with an infrared temperature probe, more than 70ºC above room temperature. Because of these large losses, an accurate energy balance cannot be performed. In addition, it is difficult to estimate the maldistribution which was created by superheating only one group of microchannels, and thus raising the pressure drop of that path above that of the unheated paths. This factor explains why the mass flow rate through Group 1 is only 7% of the total mass flow into the evaporator.

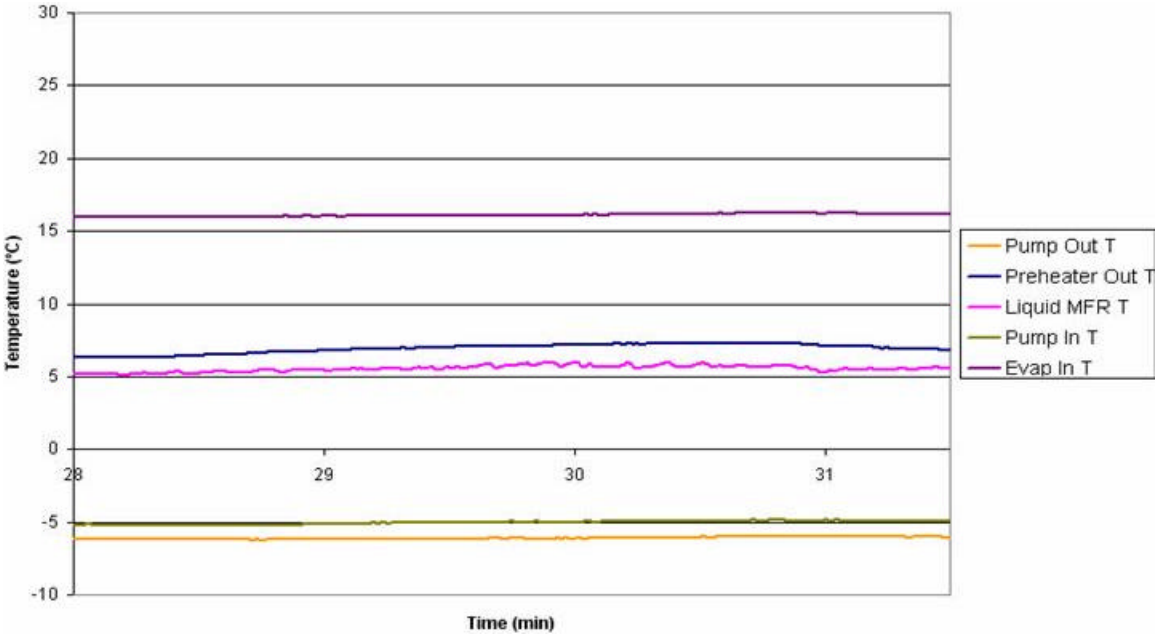

Figure 57 – Pump, Preheater, and Liquid MFM Temperatures for Group 1 heated, 20-100% Power, R134a

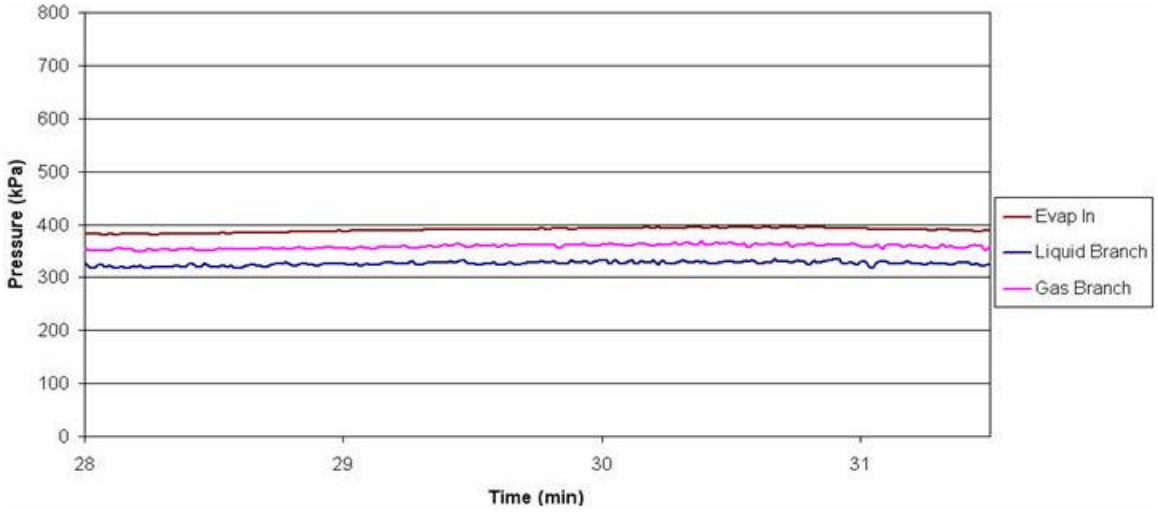

Figure 58 – System Pressures for Group 1 heated, 20-100% Power, R134a

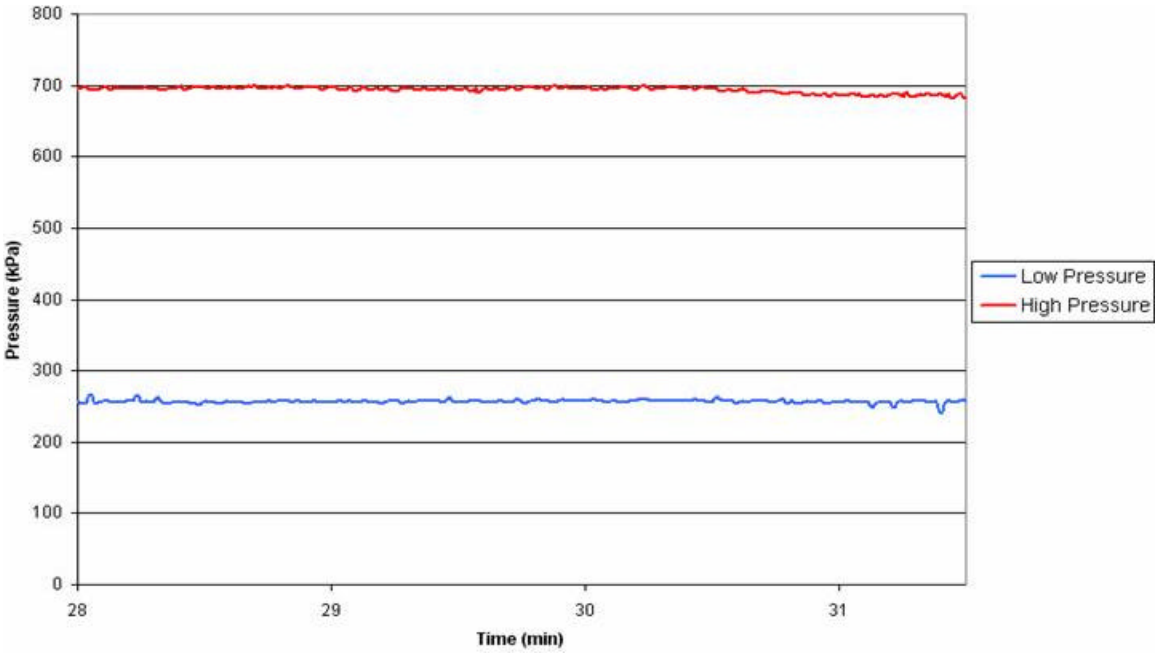

Figure 59 – Condensing Unit Pressures for Group 1 Heated, 20-100% Power, R134a

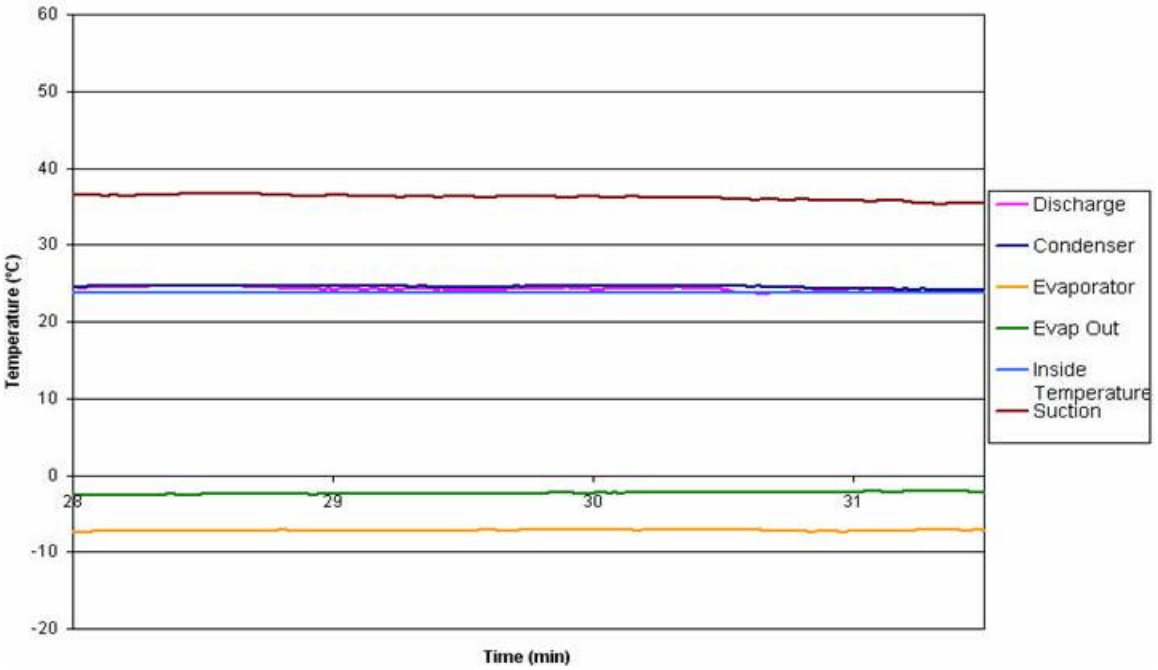

Figure 60 – Condensing Unit and Room Temperatures for Group 1 Heated, 20-100% Power, R134a

Figure 59 and Figure 60 show stable operation for the condensing unit during heating tape testing, as was observed in the first test. The condensing unit is shut off during minute 31.

The results of the second test show that the experimental system is able to measure gas and liquid mass flow rates with sufficient heating input across the evaporator. The third test is conducted with heating applied to all 10 groups of microchannels, to verify that the system can measure mass flow rates in multiple branches during the same test.

The heating input to the evaporator was controlled by setting the fractional on-time of the heating tapes to 20%. This resulted in a time-averaged heat input of 2.8 kW across the evaporator. Under this heat load, superheating occurred in several groups of microchannels, and accurate mass flow rate data for those groups was obtained. At that time, the heater controls described in Section 3.2.8 were not yet implemented, and individual groups of heating tapes could not be controlled. Instead, the control scheme only prevented the surface temperature of any microchannel at the collector header from exceeding 70ºC. If a 70ºC temperature was reached by any microchannel, power was cut off to the entire tape array.

Figure 61 and Figure 62 are plots of the mass flow rates for a 2.8 kW heat load condition, showing the individual groups which are being measured at different times. It must be noted that at certain times, the microchannels do not receive heat due to safety controls. Figure 63 shows the periods of time in which the microchannels do receive heat, and also the evaporator outlet temperatures for each group with respect to time. The only two groups which have superheated vapor at their outlets are Group 9 and Group 10. This is because these two groups receive the lowest amount of liquid flow of all the

microchannel groups, and thus have the lowest latent heat capacity. The remaining 8 groups have exiting flow which is two-phase at all times. The most critical part of the test occurs during measurement of the mass flows in Groups 10, 9, 8, and 7. The readings for the remaining groups are not reliable, due to the heating tapes being shut down, which will be discussed below.

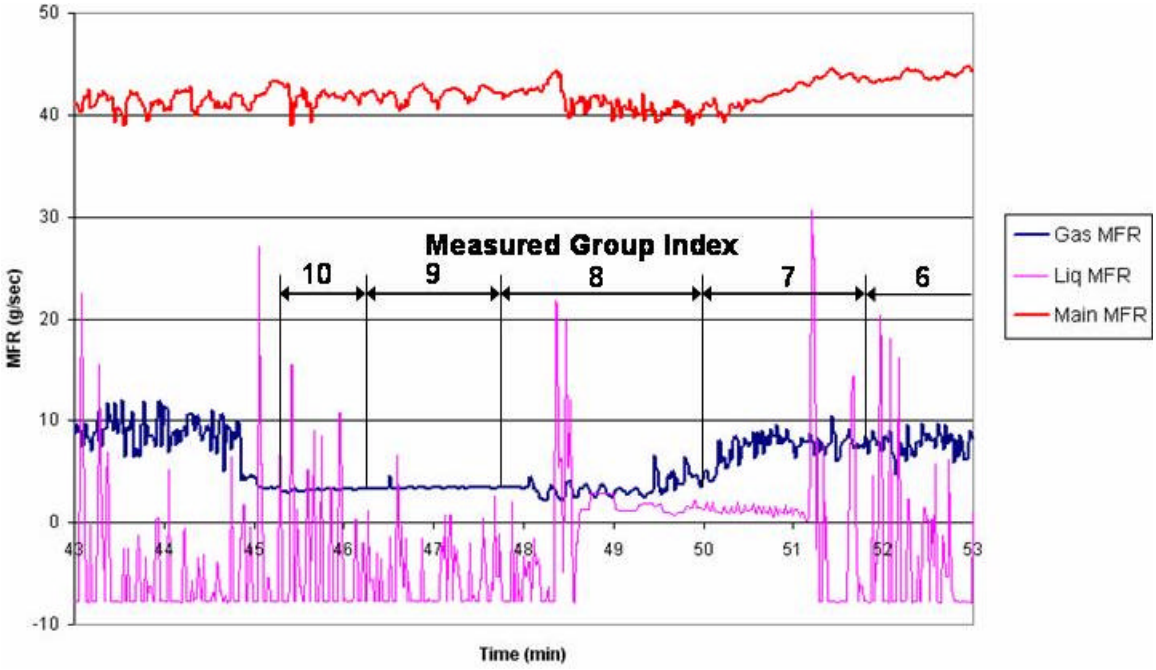

Figure 61 – Mass Flow Rates, All Groups Heated, 20% Power, R134a, (1 of 2)

Groups 10 and 9, as mentioned above, have superheated vapor at their outlets. As observed in previous tests, this results in a steady and reasonable gas mass flow rate reading for those groups. In Group 8, both the liquid and gas mass flow sensors provide fluctuating signals, which is explained by the frequent heating tape on-off cycles. The gas mass flow reading during Group 8 measurement has spikes every 10 seconds, which is the period of the heater cycles. Group 7's mass flow rates exhibit similar behavior, with more stability for the liquid mass flow rate, and more fluctuations for the vapor mass flow rate. Based on the trends from Group 10 to Group 7, it is clear that the vapor mass flow reading is most stable for superheated gas or very high vapor quality outlet flows.

Before any additional groups were measured, the heating tapes were turned off by the high temperature safety control. This change occurred during the 51st minute, and the tapes remained off for over 5 minutes until the surface temperature of the microchannels dropped below 70ºC. Figure 63 shows the transient behavior of the outlet temperature before and after the heating tapes were shut off.

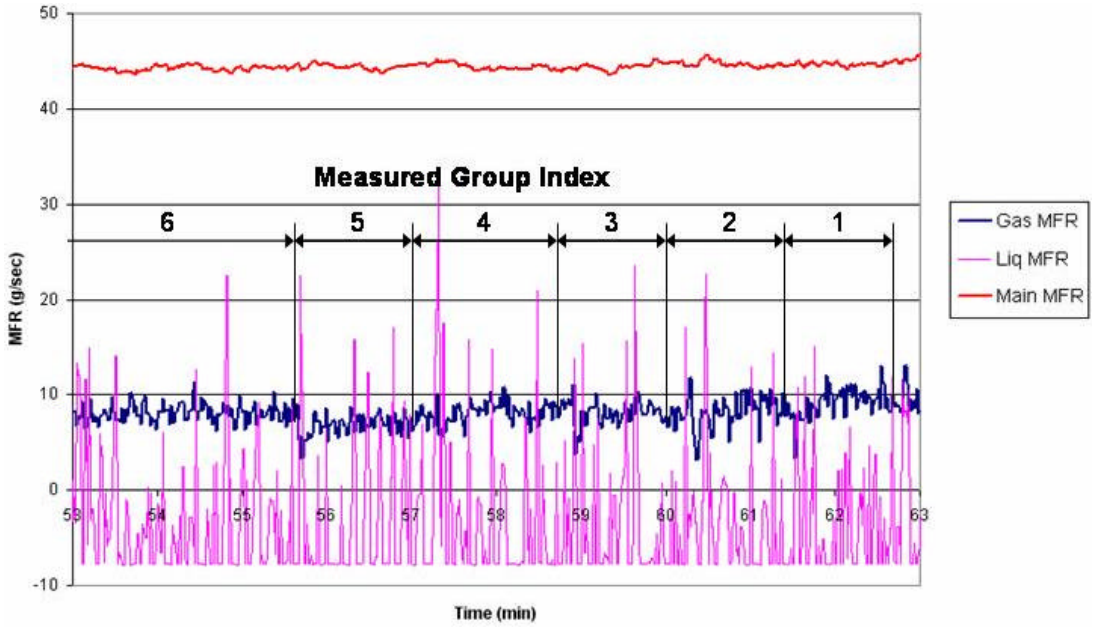

Figure 62 – Mass Flow Rates, All Groups Heated, 20% Power, R134a, (2 of 2)

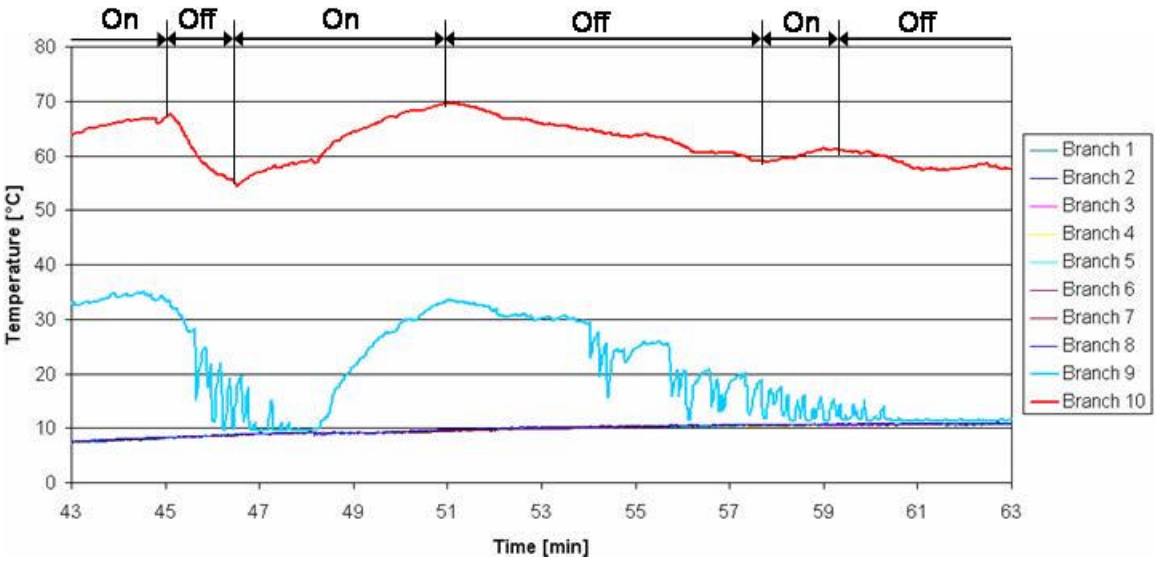

Figure 63 – Temperature Profiles of Microchannel Heat Exchanger Outlets, All Groups heated, 20% Power, R134a. On/Off Refers to Heating Tapes

The liquid and gas mass flow rates of the remaining 6 groups were not able to be measured accurately. This was because the heating input cycles were too brief to increase the vapor quality to the level necessary for a good phase separation. Figure 62 shows the mass flow data for these groups, which are not realistic. Based on the energy balance used in the first group, less than 2 g/s of refrigerant is evaporated with a 2.8 kW heat load across the evaporator, and Groups 1 and 2 are predominantly liquid at the microchannel inlets. Therefore, vapor mass flow rates of between 7 and 10 g/s are not reasonable. However, if all heater groups are controlled independently, it can reasonably be expected that the results would mirror those of Group 1 in the first and second tests of this chapter.

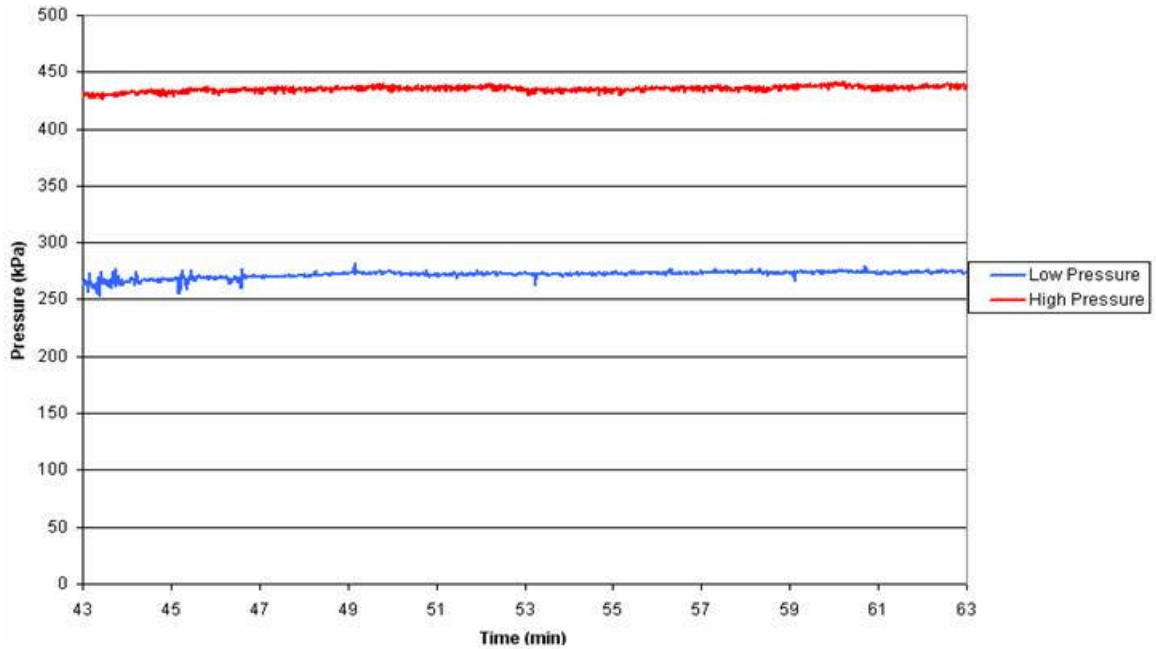

Figure 64 – Condensing Unit Pressures, All Groups Heated, 20% Power, R134a

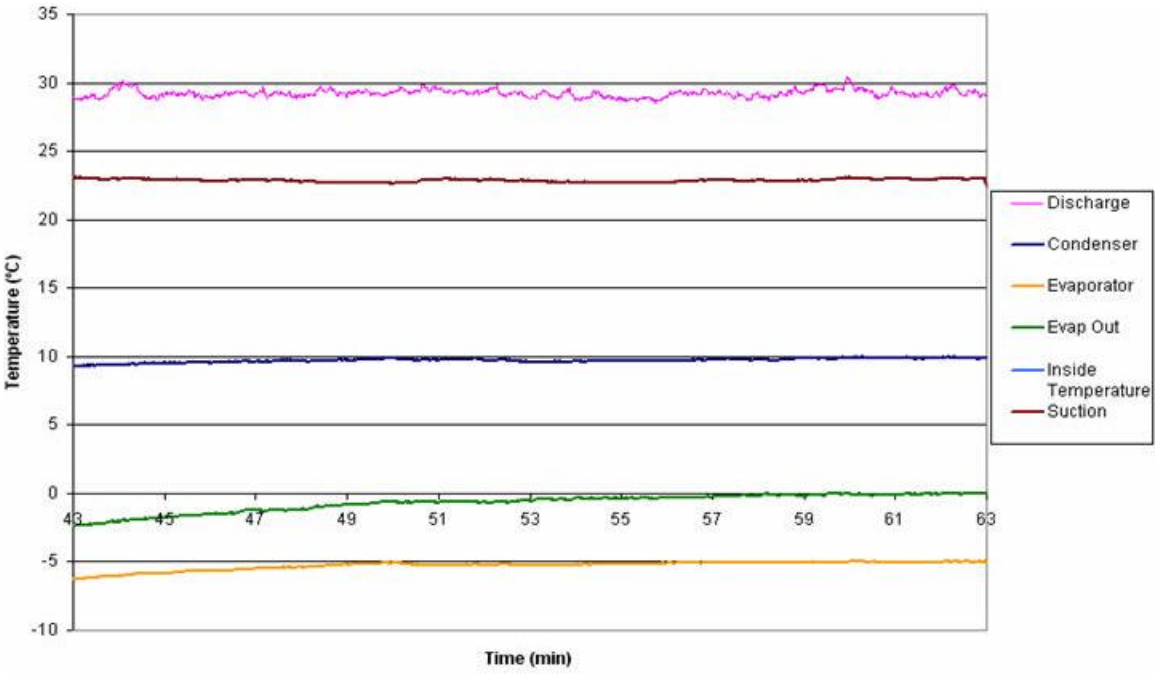

Figure 65 – Condensing Unit and Room Temperatures for All Groups Heated, 20% Power, R134a

Figure 64 and Figure 65 show the behavior of the condensing unit cycle during the third test. After turning on the heating tapes in the experimental system, neither the expansion valve nor the hot gas bypass valve were adjusted. It can be seen the evaporator inlet and

outlet temperatures rise during this time, as the condensing unit cycle responds to the new 2.8 kW heat load. However, no appreciable change is noted in the condensing unit pressures or other temperatures.

Based on these three trial runs, and the use of the heater control scheme described in Section 3.2.8, the system is able to measure maldistribution. A final note on the data in this chapter is that the differential pressure across the microchannel heat exchanger is not measured for these three data sets. The reason for this is that the original transducer was damaged, and testing continued without the sensor. At the time of this report, a replacement is installed in the system, but no test data are yet available.

7 Conclusions

The experimental setup has been shown to be operational. The following capabilities have been demonstrated by the system, through preliminary testing and video acquisition:

1) Visualization of the flow through a flat multiport header
2) Two-phase refrigerant distribution measurement in a microchannel heat exchanger

The system is unique among published works in that it can vary the geometry of the inlet header to a microchannel heat exchanger while maintaining visual access to the flow. In addition, the experimental setup can effectively measure the influence of the following parameters on maldistribution in a microchannel heat exchanger's multiport header.

1) Tube Number
2) Tube Pitch
3) Refrigerant
4) Heat Load
5) Inlet Location
6) Mass Flow Rate

8 Future Work

Since this work centers around the construction of a test facility, the most clear future work lies in completing parametric testing on flow maldistribution. The testing should include, at a minimum, variation of these parameters:

1) Tube Number
2) Tube Pitch
3) Refrigerant
4) Heat Load
5) Inlet Location
6) Mass Flow Rate

In addition, the test facility could be used to measure the impact of the following factors on flow maldistribution in a multiport header.

1) Header Orientation (vertical, horizontal)
2) Heat Exchanger Flow Direction (upward, downward, horizontal)
3) Tube Shape (microchannel, round tube, other)
4) Header Geometry (inner diameter, baffles)
5) Oil circulation ratio
6) Multiple inlets
7) Tube insertion depth

The test facility is very flexible in most respects, however the phase separation mechanism has a great deal of room for improvement. Finding a better separator, or using an energy balance to determine the quality of the outlet flows, would allow the system to conduct adiabatic tests.

9 Uncertainty Analysis

A detailed uncertainty analysis is only required for the two energy balances described in Section 3.2.7. Other measurements, including mass flow rate, pressure, and temperature, have the same uncertainty as their respective sensor. Section 1.2 contains details on the accuracies of individual sensors, which will not be repeated here.

An uncertainty analysis of the inlet quality measurement can be performed, considering the combined effects of the inaccuracy of pressure, temperature, mass flow rate, and power measurements. The program EES calculates uncertainty of measurements in the preheater energy balance, and the results are shown in Table 6. The numbers are based primarily on calibrations, where available, and secondarily on manufacturer specifications. The majority of error for all of the variables stems from the accuracy of the inlet temperature measurement.

Table 6 – Uncertainty Propagation Results for Preheater Energy Balance

Measurement	Sources Of Uncertainty	Absolute Uncertainty	Units
Inlet Enthalpy	Pressure, temperature	± 0.6704	kJ/kg
Outlet Enthalpy	Pressure, temperature, energy balance, wattmeter	± 0.7054	kJ/kg
Outlet Quality	Pressure, temperature, energy balance, wattmeter	±0.0039	kg/kg

Similarly, the measurement of quality distribution in the heat exchanger contains uncertainty. The inaccuracy of the mass flow, pressure, temperature, and power measurements are combined to find the total uncertainty in the energy balance. Table 7

shows the uncertainty values as computed by EES for the heat exchanger energy balance. In lieu of actual data, the heating tapes are assumed to have 95% accuracy.

Table 7 – Quality Distribution Uncertainty Propagation

Measurement	Sources Of Uncertainty	Uncertainty	Units
Branch Quality (vapor outlet, energy balance)	Pressure, temperature, energy balance, wattmeter, main mass flow meter	± 0.059	kg/kg
Branch Quality (two-phase outlet)	Two mass flow meters, assumes good phase separation	± 1.03 % value	kg/kg
Branch Mass Flow (two-phase outlet)	Two mass flow meters, assumes good phase separation	± 1.03 % value	kg/s

10 References

ASHRAE, 2001, ASHRAE Handbook-Fundamentals. American Society of Heating, Refrigerating and Air-Conditioning Engineers, Inc., Atlanta, GA.

Asoh, M., Hirao, Y., Watanabe, Y., and Fukano, T., 1991. Phase separation of refrigerant two-phase mixture flowing downward into three thin branches from a horizontal manifold pipe. In: ASME/JSME Thermal Eng. Proc. ASME, pp. 159–164.

Bajura, R. A., 1971. A model for flow distribution in manifolds. In: J. of Engineering for Power. pp. 7–12.

Bajura, R. A., and Jones Jr, E. H., 1976. Flow distribution manifolds. In: Trans. of the ASME. In: Gas Turbine and Fluids Engineering Conference. Paper No. 76-FE-7.

Bassiouny, M. K., and Martin, H., Flow Distribution and Pressure Drop in Plate Heat Exchangers – I. U-type Arrangement. In: Chemical Engineering Science, V. 39, 1984, pp. 693-700

Beaver, A. C., Hrnjak, P. S., Yin, J. M., and Bullard, C. W., 2000. Effects of distribution in headers of microchannel evaporators on transcritical CO2 heat pump performance. In: Proceedings of the ASME Advanced Energy Systems Division. V. 40.

Cho, H., and Cho., K., 2004. Mass Flow Rate Distribution and Phase Separation of R-22 in Multi-Microchannel Tubes Under Adiabatic Condition. In: Microscale Thermophysical Engineering, V. 8, N. 2, pp. 129-139.

Cho, H., Cho, K., Youn, B., and Kim, Y. S., 2002. Flow maldistribution in microchannel evaporator. In: Ninth Int. Refrigeration and Air Conditioning Conf., Purdue.

Fei, P., Chandrak, D., and Hrnjak, P., 2002. Refrigerant distribution in the inlet header of plate evaporators. In: SAE World Congress, Paper 2002-01-0948.

Hrnjak, P., 2004. Flow Distribution Issues in Parallel Flow Heat Exchangers. In: ASHRAE Transactions, V. 110, N. 1.

Kariyasaki, A., Nagashima, T., Fukano, T., and Ousaka, A., 1995. Flow Separation Characteristics of Horizontal Two-phase Air-Water Flow into Successive Horizontal Capillary Tubes Through T-junction. In: ASME/JSME Thermal Engineering Joint Conference, Maui, HI, V. 2, pp. 75-82.

Kim, Jong-Soo, Lee, Ki-Taek, Kim, Jae-Hong, Ha, Soo-Jung, and Im, Yong-Bin, 2004. A relation between two-phase pressure drop and flow distribution in a compact heat exchanger header. In: Second International Conference on Microchannels and Minichannels, Rochester, NY, Paper Number ICMM2004-2363, pp. 413-420.

Kulkarni, T., Bullard, C., and Cho, K., 2004. Header design tradeoffs in microchannel evaporators. In: Applied Thermal Engineering, V. 24, pp. 759-776.

Moran, M. J., and Shapiro, H. N., 1993. Fundamentals of engineering thermodynamics. John Wiley & Sons, Inc.

Oh, S. J., and Lee, K. S., 2001. Optimal Shape of Header Part in a Parallel-Flow Heat Exchanger. In: Korean Journal of Air-Conditioning and Refrigeration Engineering, V. 13, N. 10, pp. 1017–1024.

Rong, X., Kawaji, M., and Burgers, J. G., 1995. Two-phase header flow distribution in a stacked plate heat exchanger. In: ASME/JSME Fluid Engineering and Laser Anemometry Conference and Exhibition.

Sa, Y. C., Jang, D. Y., Ko, Oh, S.K., Oh, S.Y., and Chung, B.Y., 2003. Flow Mal-distribution Of Flat Tube Evaporator. In: The 4th international Symposium on HVAC, Beijing, China.

Tae, S. J., and Cho, K., 2003. Effect of geometric and dynamic parameters on the two-phase flow distribution of R-22 in branch tubes. In: Int. Congress of Refrigeration, Washington, D.C.

Vist, S., and Pettersen, J., 2004. Two-phase flow distribution in compact heat exchanger manifolds. In: Experimental Thermal and Fluid Science, V. 28, pp. 209–215.

Watanabe, M., Katsuta, M., and Nagata, K., 1995. Two-phase flow distribution in multi-pass tube modeling serpentine type evaporator. In: Proceedings of the ASME/JSME Thermal Engineering Conference. V. 2. pp. 35–42.

Wen, J., and Li, Y., 2004. Study of Flow Distribution and its Improvement on the Header of Plate-Fin Heat Exchanger. In: Cryogenics, V. 44, N. 11, pp. 823-831.

Winkler, C. M., and Peters, J.E., 2002. Refrigerant Droplet Size Measurements in Conjunction with a Novel Method for Improving Flow Distribution in Evaporators. In: Aerosol Science and Technology, V. 36, pp. 734-741.

Tompkins, D.M., Yoo, T., Hrnjak, P., Newell, T., and Cho, K., 2002. Flow Distribution and Pressure Drop in Microchannel Manifolds. In: Proceedings of 7th International Refrigeration and Air Conditioning Conference, West Lafayette, IN.

Zietlow, D. C., Campagna, M., and Dias, J. F., 2002. Innovative experimental apparatus to measure liquid flow distribution in two-phase flow occuring in the manifolds of compact heat exchangers. In: ASHRAE Transactions. V. 108, N. 2.